Master's thesis

NTNU
Norwegian University of Science and Technology
Faculty of Engineering

Sikander Mahe

DETERMINING ELECTRIC MOTOR BEARING FAULTS THROUGH VIBRATION ANALYSIS

Master's thesis in Mechanical Engineering (MIPROD)
Supervisor: Anna Olsen
Co-supervisor: Alexey Matveev
August 2022

NTNU
Norwegian University of
Science and Technology

Sikander Mahe

DETERMINING ELECTRIC MOTOR BEARING FAULTS THROUGH VIBRATION ANALYSIS

Master's thesis in Mechanical Engineering (MIPROD)
Supervisor: Anna Olsen
Co-supervisor: Alexey Matveev
August 2022

Norwegian University of Science and Technology
Faculty of Engineering

NTNU
Norwegian University of
Science and Technology

MASTER THESIS

DETERMINING ELECTRIC MOTOR BEARING FAULTS THROUGH VIBRATION ANALYSIS

Author: Sikander Mahe

Supervisor: Anna Olsen

Co-supervisor (Alva Industries AS): Alexey Matveev

AUGUST, 2022

Preface

This paper is written as the master's thesis for the final semester of the 2-year master's program "Mechanical Engineering". It is written in collaboration with Alva Industries.

Trondheim, 2022

Abstract

Is there a way to consistently predict motor failure in a flying drone? This thesis will investigate whether vibration analysis and monitoring of motor bearings can be utilized to find faults in an electric drone motor. This will be done by conducting experiments of different motor setups. By looking at the bearing vibration data from a static motor and comparing it to a motor subjected to dynamic movement, it can be determined whether a difference in vibration patterns can be established. By investigating these differences, it will give insight into whether it is possible to pick up on bearing vibrations that indicate the occurrence of failure. Literature and theory surrounding vibrations analysis is studied to ensure that the experimental work has a solid theoretical basis. An experimental setup is described, which details a way to carry out the experiment and what is needed to do so. Finally, the experiment is carried out and the resulting data is described. The results are interpreted to determine the answer to whether vibration analysis can be used to determine bearing faults in electric drone motors.

Content

List of figures

Chapter 1 - Introduction

In recent times, the prevalence of unmanned aerial vehicles (UAV) or drones have increased significantly. Drone technology has improved, and there are many use cases today, including but not limited to agriculture, photography, cargo transport, and even military missions. Drones can be found in many different sizes with varying speeds and lift, depending on the intended use-case. There are many advantages to using a drone, perhaps the biggest is the absence of an airborne pilot. This means that drones don't need to worry about the endurance of the pilot, human error will therefore be less prevalent and drone design doesn't need to be limited by the necessity of including a cockpit to contain a person. There are several different viable configurations for drones, but the two main types are fixed-wing UAVs and rotary-wing UAVs, where a common setup is the quadcopter which utilizes four propellers. With the current progress of drone technology with the usage of drones increasing, the safety and reliability of drones is as important as ever.

Reliability is central to the future development of UAVs. When it comes to commercial flight, the failure rate is around 10^{-5}while for drones it is around 10^{-3} (Enrico Petritoli, 2018). Though drones do not need to account for the safety of human lives the way that airplanes do, it does not mean that drone design cannot prioritize reliability. However, as drones continue to become more commonly used, the risk that a malfunctioning drone could pose a threat to persons on the ground or nearby objects will increase. By increasing reliability, the average lifespan and mean time to failure of a drone will also improve. As such a focus on drone reliability can lead to an improved and safer product.

One of the most important components in an unmanned aerial vehicle (UAV) is the motor. The reliability of the motor will therefore also play a big part in the reliability of the drone itself. As it is important to prevent failures that could lead to damages and safety concerns, determining whether the electric drone motor will fail or not is a matter of great importance. This paper aims to tackle this issue by looking at the bearings and analyzing vibrations from slotless electric motors. With the bearings being an integral part of the motor, a bearing failure can eventually lead to motor failure. By analyzing the bearing vibrations in the motor, could it be possible to determine if the bearings are about to fail?

1.1 Research question

The following research question should be answered:

Is it possible to consistently analyze vibration readings from a slotless electric drone motor to identify possible mechanical motor issues?

The purpose of this research question is to help determine whether it is possible utilize vibration analysis as a part of drone condition monitoring. By answering this question and possibly confirming the viability of vibration analysis, that information may be used to improve drone condition monitoring in the future.

To answer the research question, current theory is reviewed that looks at the existing literature for bearing failure and vibration analysis. An experiment is planned with an experimental setup describing the experimental work that is conducted in order to measure real vibration data and

analyze it. Additionally, the results of the experiment are analyzed and discussed to see how they relate to the project's research goals.

1.2 Background

Alva Industries AS (Alva) is a Trondheim based company that researches, develops, and produces electric motors. This project is carried out in collaboration with Alva. By researching vibration analysis, it may be possible to discover new ways for Alva to deliver a better product to their customers. If Alva can use vibration data to predict that a bearing is going to fail, that information can then be used to prevent motor failure. While vibration analysis is commonly used for industrial machinery, it is not typical to see on moving machinery like a drone. If it is possible to analyze vibrations to accurately predict motor failure of a drone in flight, then that would be highly beneficial for any drone operators.

Previously a project has been conducted with Alva for the development of a dynamic test rig for slotless motor testing . The project for this thesis aims to utilize this previous work using the test rig to perform vibration analysis. Since test rig aims to emulate the real dynamic movement of a drone in flight, this can lead to realistic vibrations for the motor bearings as well.

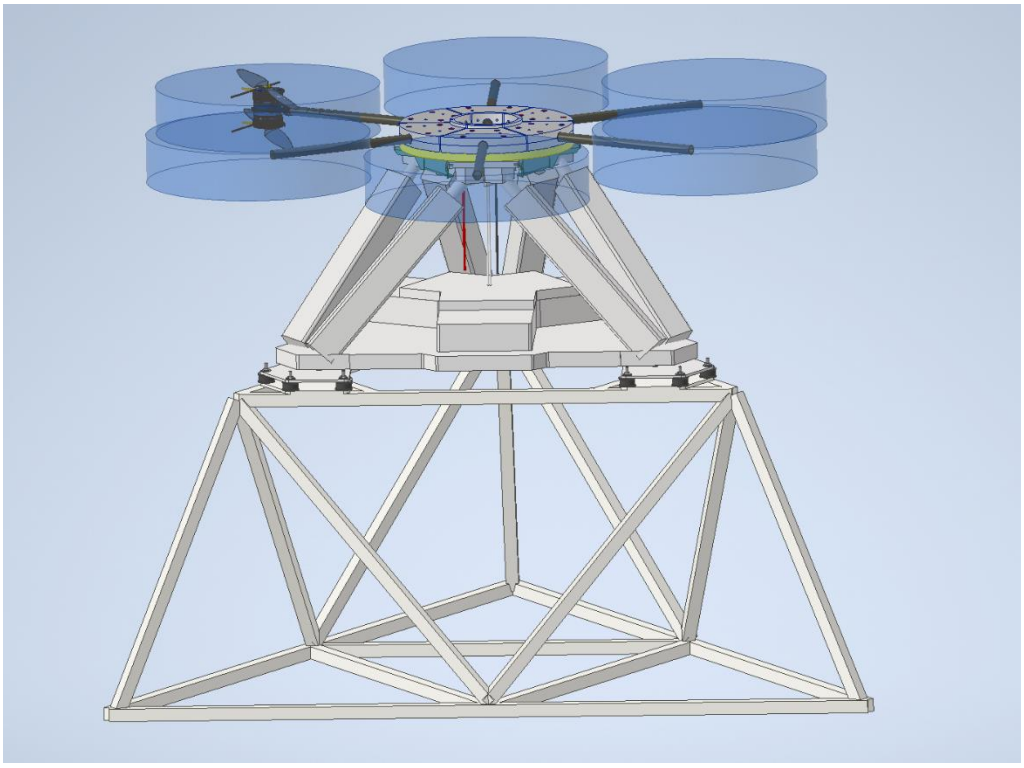

FIGURE 1 CAD DRAWING OF 6 DEGREES OF FREEDOM (DOF) MOTION RIG (COURTESY OF ALVA)

As shown in figure 1, there is a metal framework foundation that supports a 6 DOF movement platform. The movement platform can emulate real drone movement thanks to 6 actuators that can produce similar movements and speeds to that of a real drone. On top of the movement platform, bars can be connected to several motors and rotors. When the rig is running, the motors will be subjected to realistic movements and forces. This makes the 6DOF test rig an ideal environment to use for testing vibrations on the bearings as well.

1.3 Motivation and goals

The primary motivation behind this project is to explore the possibility of using vibration monitoring as a tool for condition monitoring of slotless drone motors. It is important to gain the knowledge that determines whether it is practical, or even possible to use vibration monitoring/analysis for condition monitoring in real-world conditions. This knowledge can help determine how to best build and implement a condition monitoring system, as well as provide insight into the mechanical behavior of the bearings and motors. If the project shows that it is possible, then this will be helpful for Alva as they can use this information for condition monitoring for their motors in the future. Additionally, this would make Alva's motors more appealing for customers as they would have better assurance against motor failure. Through the use of condition monitoring, Alva can aim to claim that their systems are the most reliable and have the highest availability.

To fulfill these motivations, the goals for this project are defined as:

- Determine how to get accurate vibration readings from the motor bearings
- Design an experiment capable of gathering the necessary vibration readings
- Determine if it is possible to use vibration readings to predict bearing failures

These goals provide the necessary steps towards answering the research question.

1.4 Approach

In this thesis both a theoretical and experimental approach will be utilized. A theoretical basis will be set through a review of relevant theory that mainly focuses on exploring the current literature regarding vibration analysis and bearing failure. The theory is reviewed using peer-reviewed sources. This information is to be cross referenced from multiple sources sampled from reliable journals, books, and articles. Different search terms and keywords will be utilized to examine an array of different sources.

Experimental work will also be carried out and experimental data be gathered. Utilizing previous work with Alva, a 6 degrees of freedom movement rig will be used to emulate drone movement. By having motors running in these conditions, a realistic environment for the bearings can be created. This allows for a vibration experiment with realistic conditions to be performed. As such, an experimental approach can be taken to gather realistic data that provides information which will help answer the research question. These theoretical and experimental methods will be utilized to progress towards the results that determine whether drone motor condition monitoring through vibration analysis is possible.

1.5 Limitations

The biggest limitation for the project is lack of access to a motor with faulty bearings due to a lack of time and resources. To answer the research question, it is important to be able to compare vibration readings from healthy and faulty bearings, and this is taken into account through the experimental setup. The proposed method of inducing bearing fault described in the test plan is rusting the bearings. Since a faulty motor is unavailable, the complete experiment cannot be carried out. To account for this, existing data of healthy and faulty bearing tests are used. This data is then compared to the data gathered from Alva with the healthy motor to discuss the possible effects of faulty bearings on Alva's test rig.

Chapter 2 – Theory

In this chapter the theoretical background for electric motor failure and fault detection through vibration monitoring will be reviewed. In addition, bearing vibration experiments will be studied to determine possible vibration patterns that correlate with failure. Lastly, the use of simulation to study bearing behavior is explored.

2.1 Electric motor fault types

An electric motor converts electrical energy into mechanical energy. Most electric motors work through the interaction between the motors magnetic field and electric current in a wire winding that generates force (torque). Commonly used are both AC (alternating current) and DC (direct current) electric motors. Regardless of this the electric motor uses an electric current to produce magnetic fields that generate rotational mechanical energy. Electric motors can generally be classified into the categories seen in Figure 2.

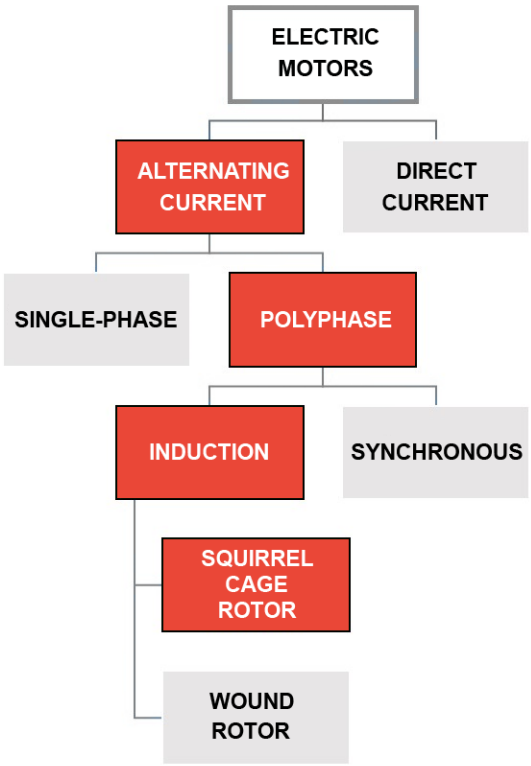

FIGURE 2 GENERAL CLASSIFICATION OF ELECTRIC MOTORS. (G. I. ELECTRIC)

Electric motor components are often categorized into five portions (Figure 3), with the most integral parts being the bearings, rotor, and stator. are also central to investigate when it comes to failure. The stator is a stationary part of the motor made of metal laminations. Electromagnetic energy is produced by the stator through the windings or permanent magnets. The windings are made from insulated metal wire and coils or winds around the rotor or stator. When energized, the windings form magnetic poles. Electric motor bearings are usually ball or roller bearings and they act as a support for the rotating motor shaft. (D. electric)

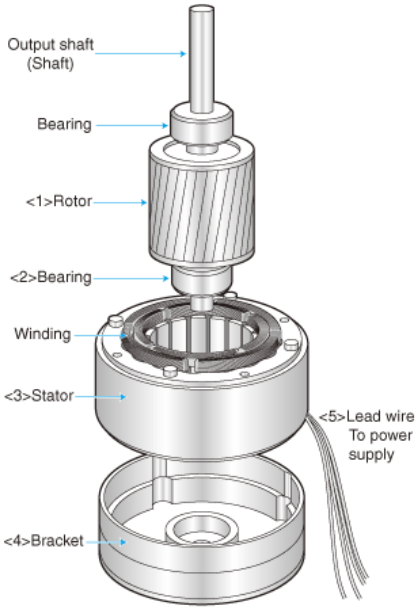

FIGURE 3 MOTOR COMPONENTS (NICDEC)

Electric motor failures can be categorized into 3 types of failure: electric, mechanical and magnetic failures. In the following sections some common faults will be described.

Electric faults

Electrical faults in an electric motor are usually related to the windings (Figure 4). The windings will usually fail due to the insulation breaking down. It is vulnerable to thermal, electric and mechanical stress, especially when the insulation ages as it can become weaker over time. In addition, exposure to moisture and dust can also have a degrading effect on the insulation. Electric failures often lead to short circuiting. (Kallaste, 2021)

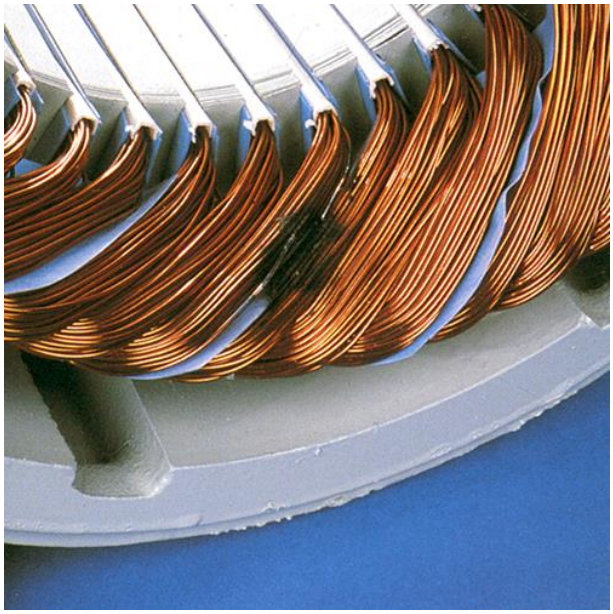

FIGURE 4 INSULATION FAILURE CAUSED BY SHORTED WINDINGS(ESEA, 2019)

Mechanical faults

The primary mechanical faults are bearing failures, which account for ~40% of all electric motor faults. This means that bearings the primary cause of failure in electric motors. (Robbersmyr, 2017) Bearings can commonly fail due to poor lubrication, wear, corrosion, misalignment, and fatigue from stress. Ball bearing failure commonly occurs in the form of indentation(brinelling) (Figure 5). Failure can occur in the outer/inner race, rolling elements and bearing cage (Figure 6).

FIGURE 5 INDENTATION(BRINELLING) ON BEARING RACEWAY. (LANGNAU, 2013)

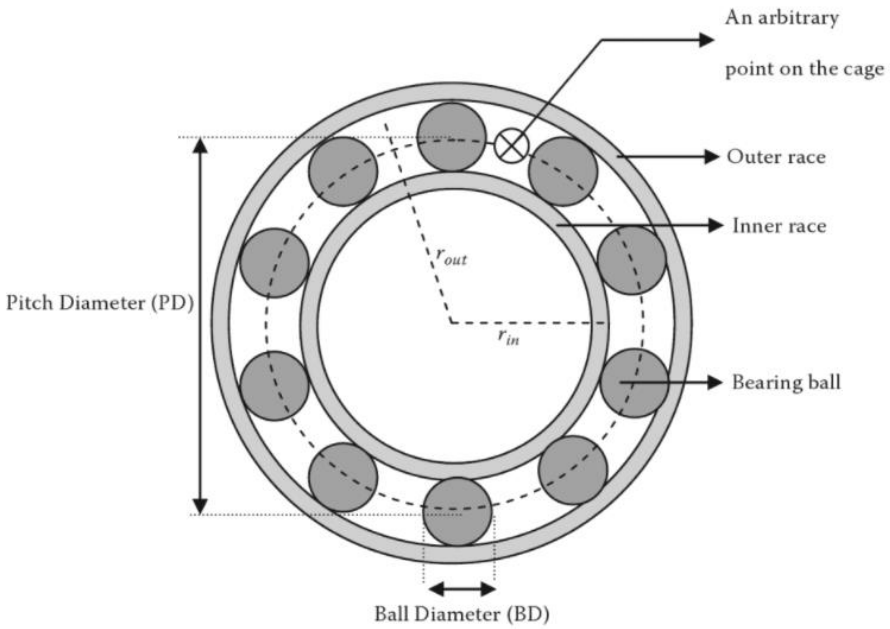

FIGURE 6 2D BEARING DIAGRAM. (HOMAYOUN MESHGIN-KELK, 2012)

Another mechanical fault that can occur is eccentricity. This is when the air-gap between the stator and rotor is uneven. This can cause varying magnetic flux which can lead to imbalance in the current flow.

Magnetic faults

The most common magnetic fault is demagnetization, which causes the magnet to wholly or partially lose its magnetic field. Common causes for this are overheating and short-circuiting within the motor. In addition, the magnet could lose some of its effect due to corrosion or simply due to ageing. (Krishnamurthy, 2011)

2.1.1 Bearing failure

Given normal operating conditions fatigue failure starts with smaller fissures below surfaces of the raceway (surfaces of inner and outer ring) and rolling elements. These fissures then gradually propagate towards the surface. Continued stress on the bearing can also cause material flaking and cracking which can lead to uneven loads and lubrication contamination. If the lubrication is contaminated with particles, that can lead to sanding/abrasion when the abrasive particles hits the bearing surfaces. (Bartfield, 1995)

Bearing problems may also surface due to improper installation. These are often caused by the bearing being forced into the shaft or housing (Figure 7). This can lead to deformations and indentations in the bearing raceway

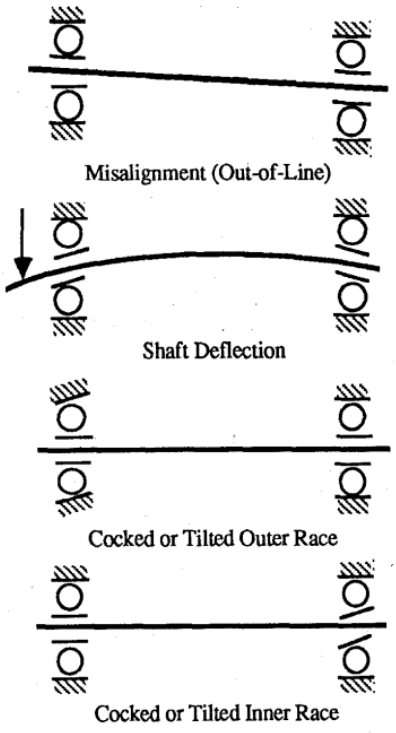

FIGURE 7 FOUR BEARING MISALIGNMENT EXAMPLES. (BARTFIELD, 1995)

2.2 Bearing fault frequencies

As previously mentioned, a bearing consists of an outer and inner race, a cage and rolling elements. Defects in each part will have their own characteristic vibration frequencies. The bearings will exhibit different frequencies based on the level of degradation. These levels of degradation can be split into 4 stages. Initially high frequencies of 5-40 kHz may be observed in the components. At the second stage frequencies of 1-5kHz also appear, and at the third stage low frequencies of <1kHz will appear. The fourth stage indicates complete bearing failure and will lead to a noisy vibration spectrum. (Robbersmyr, 2017)

The different characteristic frequencies for each part of the bearing (given an angular contact ball bearing in which the inner race rotates and the outer race is stationary) can be described as:

Train/cage frequency (FTF):

$$FTF = \frac{S}{2}\left(1 - \frac{B}{P}cos\Phi\right)\text{[Hz]} \quad (1)$$

Outer race ball pass frequency(BPFO):

$$BPFO = \frac{SN}{2}\left(1 - \frac{B}{P}cos\Phi\right)\text{[Hz]} \quad (2)$$

Inner race ball pass frequency(BPFI):

$$BPFI = \frac{SN}{2}\left(1 + \frac{B}{P}cos\Phi\right)\text{[Hz]} \quad (3)$$

Ball spin frequency(BSF):

$$BSF = \frac{SP}{2B}\left(1 - \frac{B^2}{P^2}cos^2\Phi\right)\text{[Hz]} \quad (4)$$

Where B is the ball diameter [mm], P is the pitch diameter, N is the number of rolling elements and S is the shaft rotation rate [Hz]. Disrepancies from these formulas may arise when the bearings carry significant thrust loads or if there is slippage. (Dai, 2003)

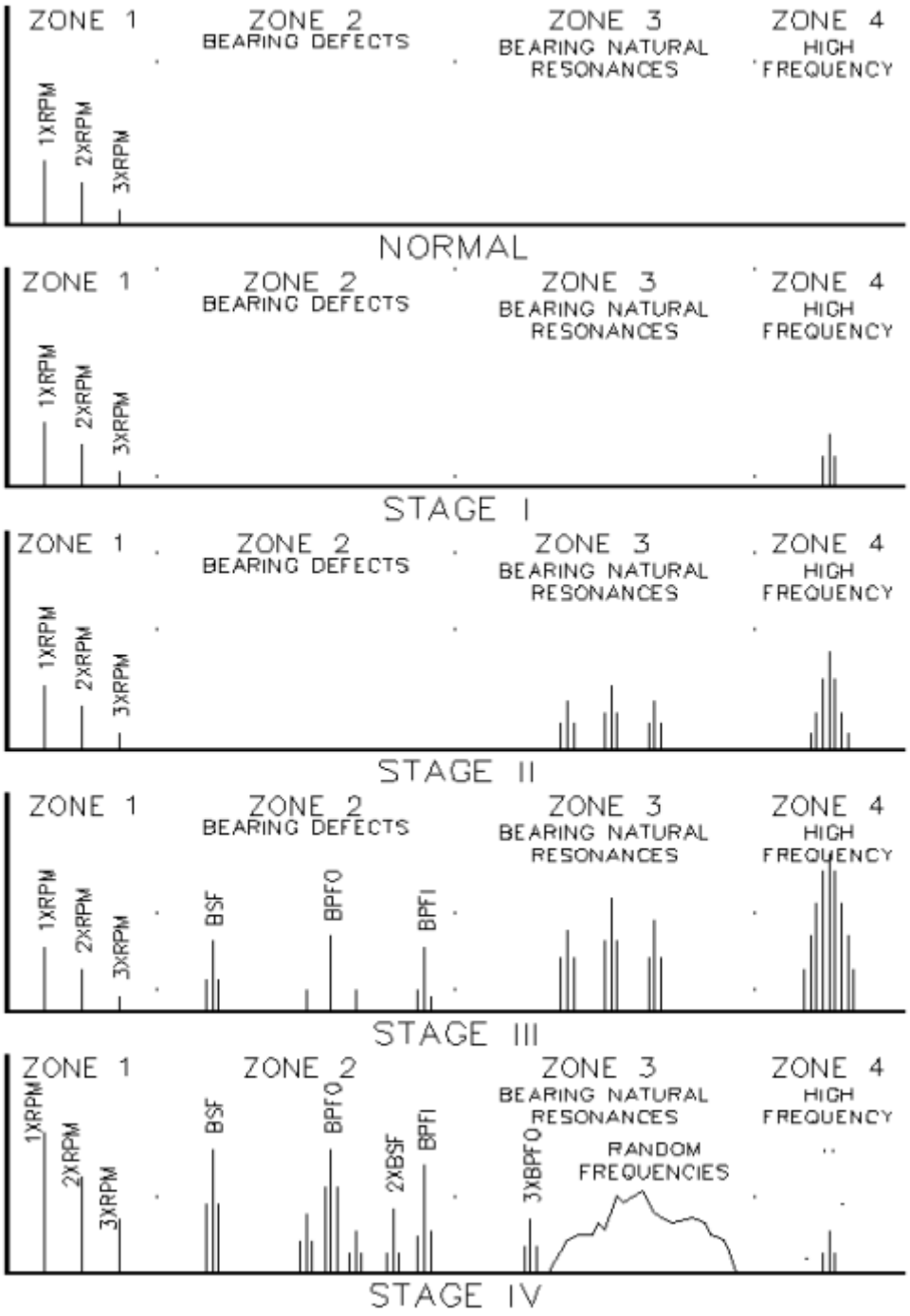

FIGURE 8 CHARACTERISTIC DISTRIBUTION OF FREQUENCIES FOR THE DIFFERENT STAGES OF BEARING FAILURE. ("STI FIELD APPLICATION NOTE," 2012)

Looking at the failure stages (Figure 8), the natural frequencies of the different bearing parts start to manifest as the bearing failure progresses. They start to appear at stage 2 and amplify during stage 3, with the characteristic frequencies for the bearing parts also appearing for stage 3, depending on the quantity of defects present on each part. The prevalence of high frequency vibrations continue to increase leading up to stage 3. At stage 4, the bearing is nearing catastrophic failure and high frequency vibrations decrease in favor of random frequencies. At stage 4 degradation in the bearing can reach a point where the internal clearances increase, which allows for the bearing shaft to rotate and move more freely. This can lead to increase in

frequencies related to unbalance and misalignment as well. Despite a decrease in high frequency values in stage 4, the quantity of high frequency values may actually spike just before complete failure. (Reuben Lim Chi Keong, 2014)

2.3 Vibration

Vibration analysis is one of the most successful techniques used for condition monitoring of rotating machines and it is an efficient and convenient tool for diagnosing mechanical problems in electric motors. (Tsypkin, 2017)

To gather vibration data vibration sensors are used. There are sensors that can monitor velocity, displacement, and acceleration. One of the most commonly used sensors for vibration measurements are piezoelectric accelerometers. These accelerometers utilize the piezoelectric effect of certain materials to measure dynamic mechanical changes such as shocks or vibrations. This is done by using a piezoelectric crystal, which will produce an electric charge when subjected to a mechanical force. The amount of charge produced is proportional to the applied force, as such this charge can be converted with electronics to determine the magnitude of the force. (Arar, 2022)

Some of the benefits of using a piezoelectric accelerometer include a wide frequency range, large variety of options for different purposes, and the acceleration signal can be integrated to provide velocity and displacement.

2.3.1 Reading vibration data

After gathering vibration data through a sensor, the data needs to be analyzed. Some of the vibration analysis parameters are acceleration, displacement and velocity. Each of these parameters emphasize different frequency ranges and be used in conjunction to diagnose issues (Table 1). Another important value is the root mean square – RMS. The RMS is directly related to the energy content of the vibration profile which gives an insight into the destructive capabilities of the vibrations. The RMS is calculated by taking the peak amplitude A and multiplying it with 0,707, which is the square root of the peak amplitude divided by 2.

$$RMS = \sqrt{\frac{A^2}{2}} \approx 0.707A \tag{5}$$

Table 1: Use cases for different vibration measurement parameters (Sensegrow, 2020)

Overall Measurement	**Application**	**Where to use it?**
Displacement Peak to Peak	Used for analyzing stress-related defects occurring in orders of rotating frequency.	Displacement is a good measure for low-frequency vibration and is not suited for high-frequency vibration. It can be used for analyzing frequencies of less than 20Hz. It can be used on equipment running up to 1200 rpm.
Velocity Peak	Used for analyzing fatigue-related defects occurring in orders of rotating frequency.	Velocity is a good measure for medium frequency vibration. It can be used in the 10Hz (600 Cycles per minute - CPM) to 1KHz (60,000 CPM) frequency range. It can be used on equipment running from 1200 to 3600rpm.
Acceleration True Peak or High-Frequency Accelerations RMS	Used for analyzing force related defects occurring in the high-frequency band.	Acceleration is a good measure of high-frequency vibration. It can be used for analyzing frequencies of more than 1KHz (60,000 CPM). It can be used for identifying bearing, cavitation, and lubrication issues.

There are several ways to analyze the vibration data. The common ways of presenting data are the time-domain and frequency domain of the vibration signals. Time domain shows the vibrations as waves on an xy-graph where y denotes the wave amplitude and x is the time period. The frequency domain shows the frequency spectrum with the amplitudes in the y-axis and frequency in the x-axis. Beyond this there are many analysis techniques that are utilized. Some of the most commonly used are “Fast Fourier Transform” – FFT and “Power spectral density” - PSD. (Hanly, 2018; Trout)

2.3.1.1 Fast Fourier Transform (FFT)

FFT is an implementation of the discrete Fourier transform - DFT algorithm using that calculates vibration amplitude as a function of frequency. DFT can be used to convert a signal from the time domain to the frequency domain. FTT does it faster by utilizing computational algorithms. Since the vibration measurement parameters of displacement, velocity, and acceleration are given in the time domain, FFT is useful to convert the measurements to the frequency domain. (Collins, 2019)

The formula for DFT is as follows:

$$x_k = \sum_{n=0}^{N-1} x_n \cdot e^{-\frac{i2\pi}{N}kn} \tag{6}$$

Which transforms a sequence of N complex numbers x_n into another sequence of complex numbers x_k (Patrick Corn, 2022)

In a steady state operation, the frequencies can be assumed to be constants and constant time sampling rates may be utilized. This is where FFT is best used, however it is less suitable to be used for variable speed/load operations since the frequencies change over time. Another technique must be utilized to see how the frequencies change over time: Short Time Fourier Transform (STFT). This splits the time sampling into smaller periods (bins) and the Fourier transform can be performed separately on these shorter timeframes. The smaller the timeframes/bins, the higher the resolution of the data (but higher resolution requires more processing). (Jagath Sri Lal Senanayaka & Robbersmyr, 2018)

2.3.1.2 Power spectral density (PSD)

Power spectral density (PSD) is also a helpful analysis tool as it can be used to characterize random vibration signals. A PSD is a measure of a signal's power content in relation to the frequency [g^2/Hz]. A PSD can be computed by multiplying each frequency bin in an FFT by its complex conjugate, which returns the amplitude in g^2. This method normalizes the amplitude value to the frequency bin width, which allows for the data to be overlaid and compared regardless of the data measurement resolution (bin widths). (Hanly, 2018)

2.3.2 Identifying failures based on vibration readings

Looking at the data from a bearing vibration experimental setup (Figure 9) where vibrations readings were taken from a healthy (a) bearing and a corroded bearing (c) (as well as tempered(b), damaged separator(d) and no lubrication(e)) a clear distinction is noticeable form the readings. Each bearing is set up with three-axis mounted accelerometers.

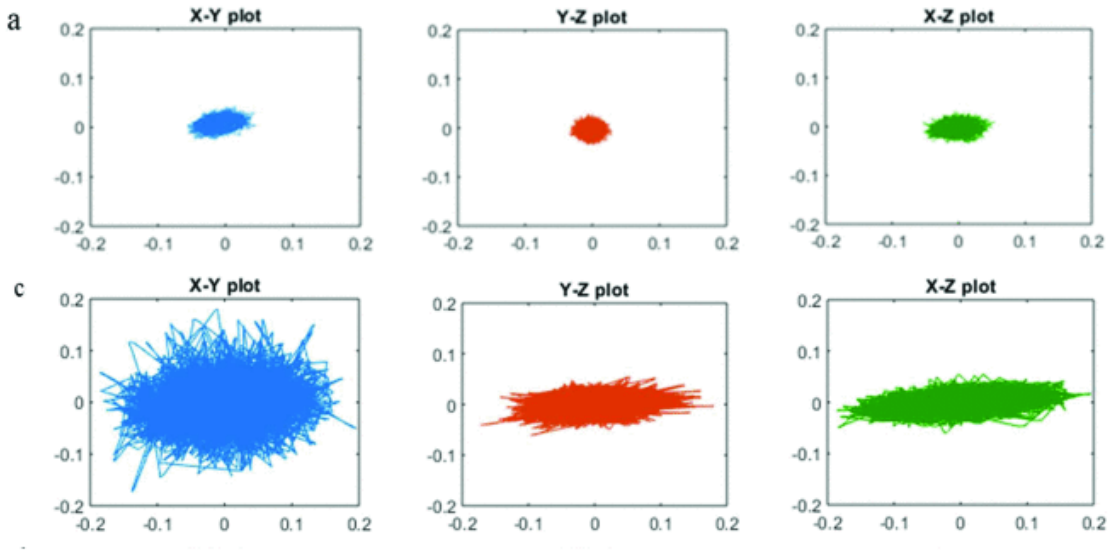

FIGURE 9 VIBRATIONS PLOTS OF A HEALTHY (A) AND CORRODED BEARING (C) IN THE XY, YZ AND XZ AXIS (KALLASTE, 2021)

Looking at figure 9 it is apparent that the corroded bearing (c) shows higher vibrations readings in all axes than in the healthy bearing (a), especially in the x-axis. Though the corroded bearing shows the most extreme difference, a similar distinction in vibration values can also be found between the other faulty bearings (b, d and e).

In another test four bearings are connected to a 2000RPM rotating shaft (Figure 10). The shaft is subjected to a 2700kg radial force while it rotates. Four accelerometers collect vibrations signals at a 20kHz frequency every 10 minutes.

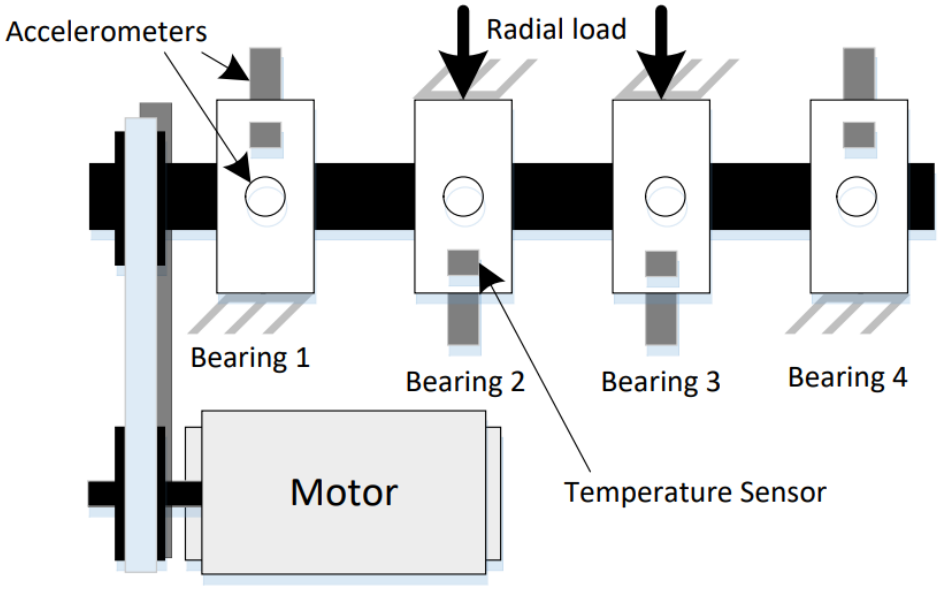

FIGURE 10 VIBRATION TEST EXPERIMENTAL SETUP WITH 4 BEARINGS (ROBBERSMYR, 2017)

At the end of the test inner, outer and rolling element failures are observed. Figure 11 shows the vibration values through the bearing lifespan.

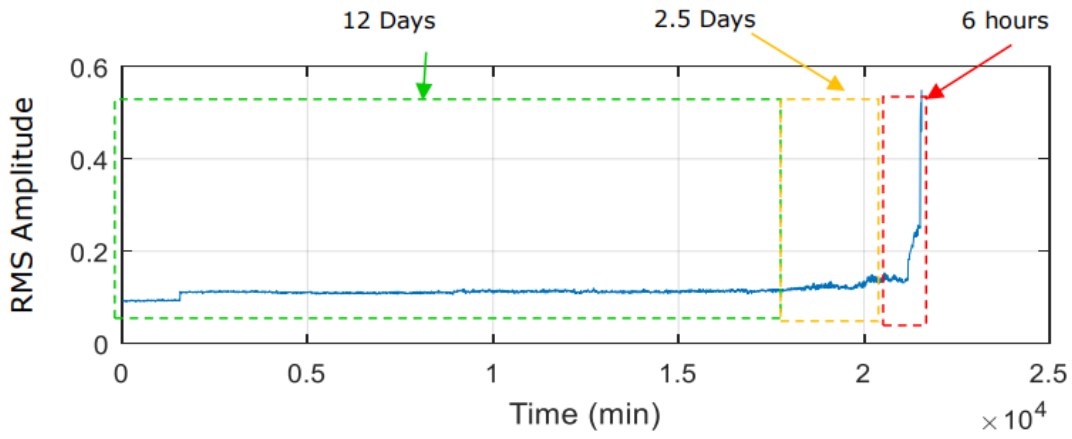

FIGURE 11 RMS OF VIBRATION SIGNAL FOR AN INNER-RACE FAULTY BEARING (ROBBERSMYR, 2017)

After 12 days the bearing starts to show signs of degradation. This continues before failure starts occurring in the final 6 hours.

2.4 Roller bearing simulation

Doing real-life experiments to observe bearing behavior might not always be practical. A lot can also be gathered from utilizing simulation methods to analyze bearing behavior. By examining the relevant literature, methods to achieve vibration simulation of bearings will be explored. Some of the commonly used simulation methods are numerical analysis, Finite element analysis/method – FEA/FEM and machine learning algorithms.

2.4.1 Literature search

When searching for data about bearing simulation a variety of search terms and sources were used. To illustrate this process, a table is shown (Table 2). General search terms were utilized in the literature search, for example “Bearing vibration simulation”. The purpose of this review is to try and determine an overview of engineering simulations for roller bearings. As such it is conducive to use general terms within the subject to broaden the possibilities of finding relevant sources. There wasn’t an abundance of relevant texts for any one search, so it was important to explore multiple combinations of keywords to try and many promising source possibilities.

Table 2: Overview of search terms used to gather sources for simulation literature

Search engine	Keyword 1	Keyword 2	Keyword 3	Keyword 4	Number of results
Google Scholar	Bearing	Vibration	Simulation		387 000
Scopus	Bearing	Vibration	Simulation		4534
Oria	Bearing	Vibration	Simulation		144
Google Scholar	Bearing	Vibration	Simulation	Ansys	21 800
Scopus	Bearing	Simulation			25 495
Oria	Bearing	Simulation			254 654
Google Scholar	Bearing	FEA/FEM	Simulation		104 000 / 93 600
Google Scholar	Bearing	Vibration	FEA/FEM	Simulation	29 100 / 42 900
Google	Roller	Bearing	Simulation		6 670 000

Google Scholar, Oria and Scopus were used as search engines. The most relevant results were found with Scholar. Oria and Scopus tended to have more results that were full books and the more relevant sources for finding simulation examples were from articles. Even if the source is quite specific into a certain subject, they can still be relevant in regard to providing examples and general info about roller bearing simulation.

Searching specifically for the program “ANSYS” was also attempted, which is, among other things, a FEA program. The idea was that searching for a specific software that could do FEA would provide more relevant results towards FEA simulation. However, searching with a specific software (ANSYS) led to significantly more pay-walled results. As such it was better to just use the generic terms FEA/FEM instead. Despite meaning basically the same thing, FEA/FEM provided different results based on which one was used. Therefore, it was important to use both terms to cover all bases. Finally, a standard Google search for “roller bearing simulation” was conducted which was successful in finding a multitude of sources on the matter. Not all were relevant or trustworthy, but there was a large number of results which lead to finding a lot of valuable information after some scrutiny of the results.

When investigating different sources, the highest emphasis was put on the introduction/abstract, simulation chapters and conclusion. These chapters usually have the most relevant information for the purposes of reviewing simulation details. What is most important to capture is the simulation process the authors conducted. Introduction gives an insight into what the purpose is, and the conclusion gives an insight into whether the simulation was successful.

2.4.2 Finite element simulation

Finite element analysis/method – FEA/FEM can be utilized to create a simulation of a bearing system. FEA allows the user to mesh the different parts of a system and simulate them getting exposed to forces or movements. A good example of FEA being used for bearings is the following simulation, which analyses the vibration data from a simulation of a defective roller bearing (Figure 12) (Gu, 2010)

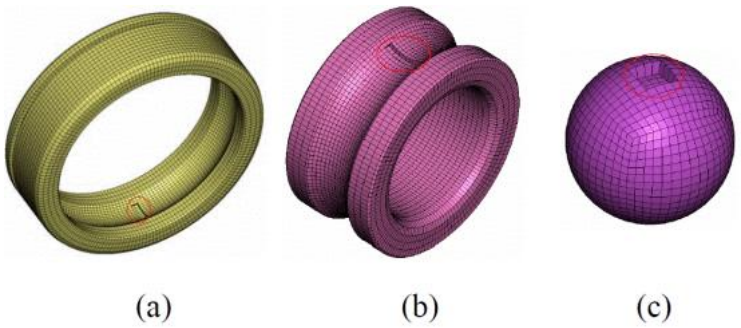

FIGURE 12 SIMULATED FAULTS ON OUTER (A) AND INNER (B) RINGS AS WELL AS ROLLING ELEMENT (C) (GU, 2010)

Local defects are simulated for each part of the bearing using the FEA program "LS-DYNA".

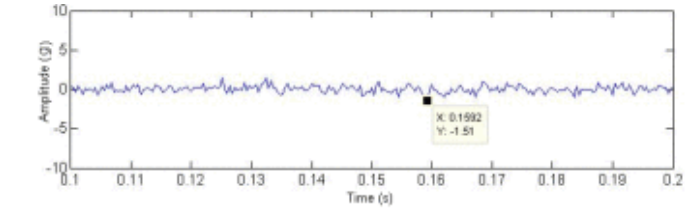

(a) The acceleration curve of healthy bearing

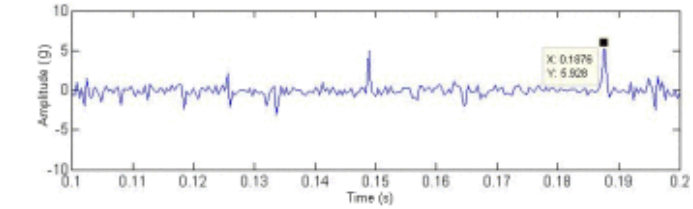

(b) The acceleration curve of bearing with defect on the outer ring

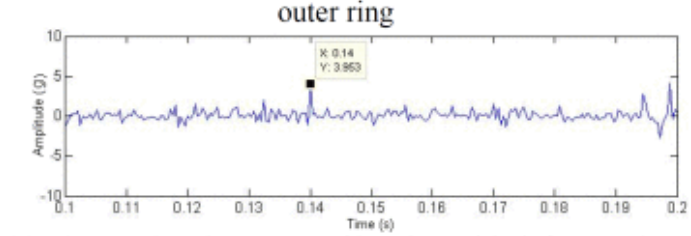

(c) The acceleration curve of bearing with defect on the inner ring

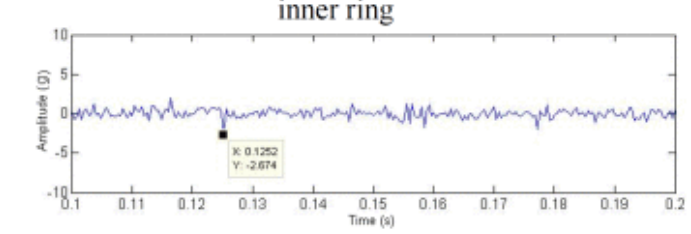

(d) The acceleration curve of bearing with defect on the rolling element

FIGURE 13 TIME DOMAIN FREQUENCY OF THE DIFFERENT SIMULATIONS A, B, C AND D. (GU, 2010)

The simulations are run, and the vibration data (Figure 13) is compared. The vibrations are based on the housing structure of the bearing, as such the most noticeable of the faults is the outer ring defect as it is closest to the housing. Regardless, a clear difference in vibrations is noticeable for all faults compared to the healthy bearing case.

Additionally, FEM simulation can also be used to assist machine learning. An example of this is using FEA to provide samples to support vector machines – SVM, which is a machine learning method. It may be difficult to provide real-world samples of many different types of faults. Therefore, the missing machine learning training samples can be provided through FEM simulation by executing the simulation and feeding the resulting time-domain vibration data.

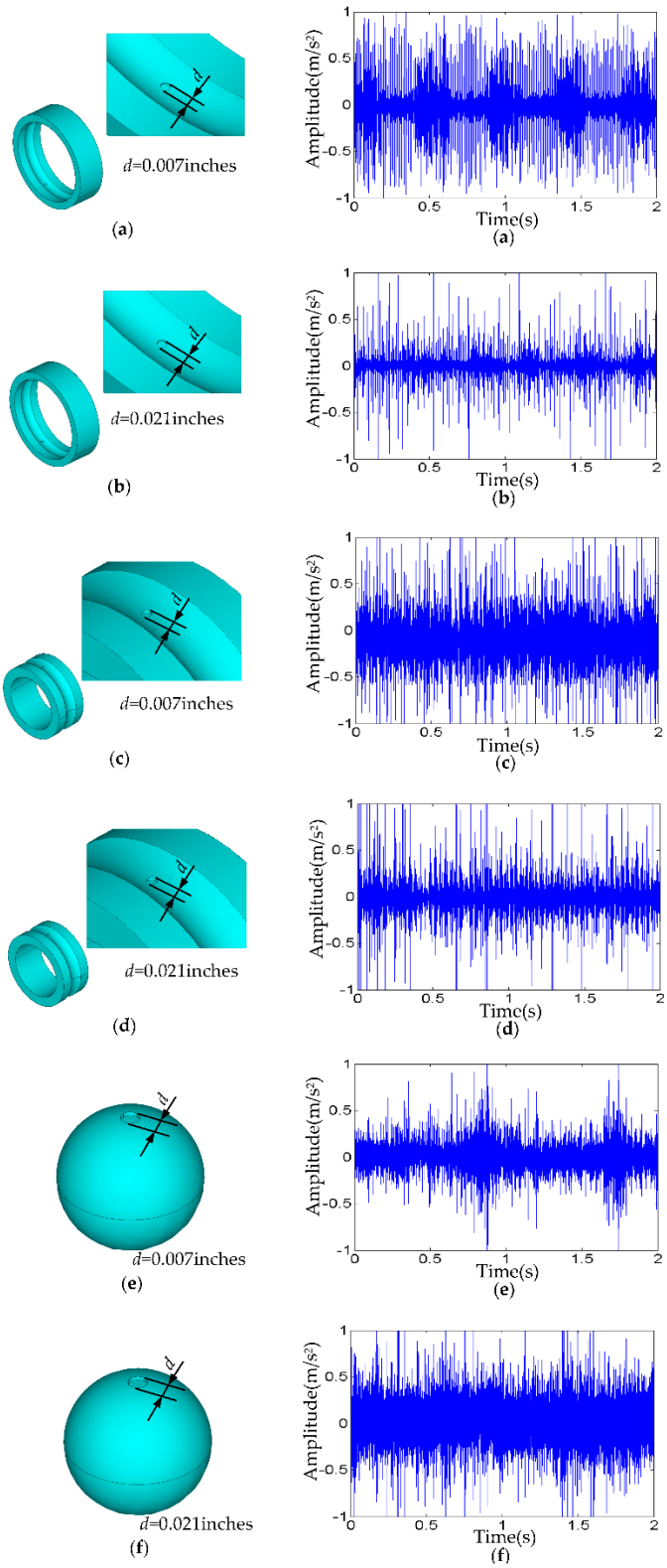

FIGURE 14 6 DIFFERENT SIMULATED FAULTS AND RESULTING TIME DOMAIN VIBRATION GRAPHS (LIU, 2019)

As shown in Figure 14 a variety of faults can be tested. FEM allows for specific faults to be tested and produces resulting vibration for each fault. This allows for a variety of samples to be fed to the machine learning algorithm that might have been impractical to gather through real world experiments.

2.4.3 Bearing simulation compared to real world experiments

Can the results gathered from a simulation experiment be trusted to be accurate in relation to a real-life experiment? This is tested and illustrated in a paper by Xin Zhang et al (Xin Zhang, 2020) where experimental and simulation results are compared. A roller bearing is subjected to the same fault in both a simulation model and a real test rig. The chosen fault is a Ø1.2mm hole on the roller element, where the real-life defects are fabricated by a laser etching technique.

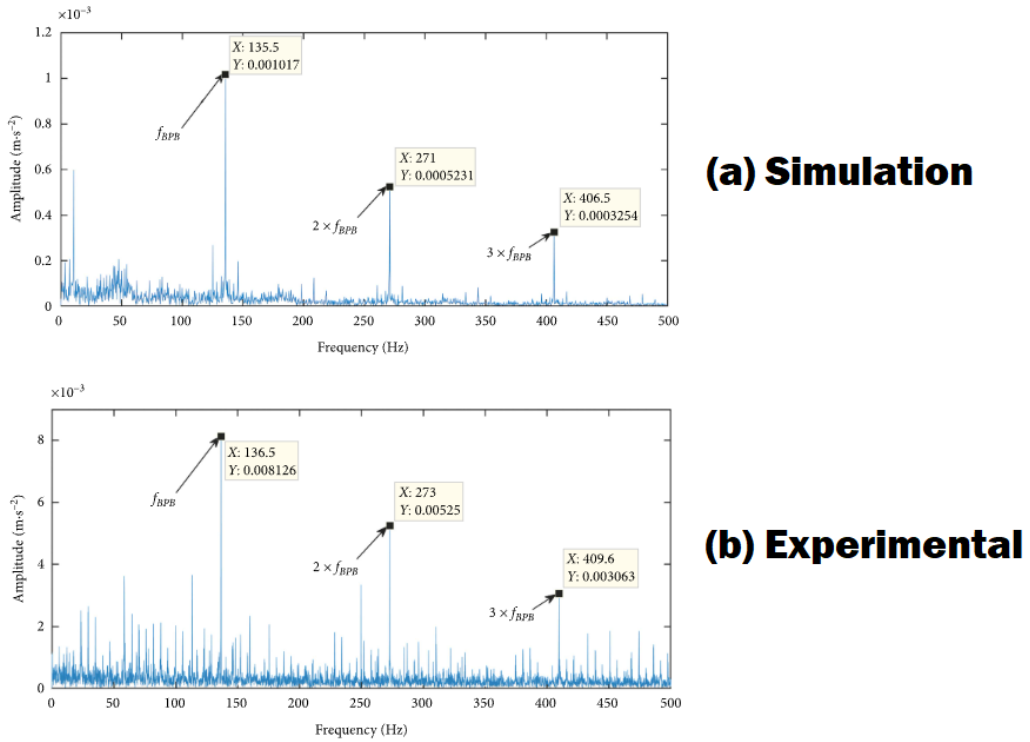

FIGURE 15 COMPARISON OF FREQUENCY DOMAIN VIBRATION (F_{BPB} = CHARACTERISTIC FREQUENCY OF ROLLING ELEMENT) OF SIMULATION RESULTS (A) AND EXPERIMENTAL RESULTS (B) (XIN ZHANG, 2020)

As shown in Figure 15, the characteristic fault frequencies found in the simulation and experimental results are quite similar. This shows that when a suitable simulation model is utilized, the results are very similar to real-life experimental results.

Simulating bearings with a 3D bearing model can be quite precise, however the drawback is that simulating the bearing in this manner is quite time and resource intensive. The 3D roller bearing model consists of many elements and nodes, so a lot of interactions have to be computed when doing a simulation. There are alternatives to the 3D model, namely a global stiffness model and a substitution model. The global model looks at the global stiffness for the entire bearing. This model is a lot more efficient, but it isn't as precise as other methods due to the simplifications. The substitution model takes elements of the bearing and substitutes them for

something equivalent but simpler with fewer elements and nodes. An example of this would be changing the rolling elements for spring elements when simulating in-plane forces for the bearing. While this method requires less computational power and is quite precise, it also requires a high level of knowledge and time to implement correctly. (Feuchter, 2021)

2.5 Future of condition monitoring and predictive maintenance

Utilizing condition monitoring (CM) on UAVs may become the norm in the future as the maintenance techniques evolve and improve. The global predictive maintenance market is expected to grow by 26.5% annually from 2021 to 2027 (Markets, 2022). What does the future of maintenance, specifically CM and by extension – predictive maintenance, look like? Implementing condition monitoring can pose a challenge when it comes to time, knowledge and resources, however as CM develops and progresses, the barrier to entry decreases as well.

Predictive maintenance is based on measuring and gathering data to predict possible failure. Commonly used is an IoT (Internet of things) network of sensors and AI/ML (Artificial intelligence and machine learning) as this allows for a large amount of data to be analyzed quickly. The IoT solution gathers the data and the ML algorithm will analyze it to identify possible faults. While an efficient method that can significantly reduce maintenance costs, it can be challenging to set up (Fant, 2021). It takes significant time to gather the necessary data and a lot of data has to be gathered and analyzed by the ML algorithm to train it and provide the ability for it to accurately detect faults. The systems that can benefit from CM are complex and have many possible failure modes, not to mention that setting up and running these processes smoothly will likely require some trial and error.

On way to make CM easier to adapt is through the use of physics-based models. This can be done by utilizing a digital twin, which is a virtual representation of an object or process. The physics-based model can be used to simulate the real-world counterpart by using data gathered from the real part. Combining this with a data driven approach can make the process of adapting CM much faster. This is due to it not only being more efficient, but with physics-based modelling, previous work done by others can also be utilized. Since there are already existing physics models of different kinds of equipment, these can be utilized to integrate the physics model into an existing system more efficiently. (Eklund, 2022)

Some companies may find it difficult to overcome the initial bottleneck of gathering the required knowledge and resources to implement a predictive maintenance program. However, there are currently solutions offered by different companies which can make the transition easier, or a lot of the work for you. One of the ways to do this is to utilize digital twins, that way the customer can send CM data of their machinery to the company, which then inserts the data into digital twins and/or other predictive maintenance software to predict failere based on real-world data.

Using predictive maintenance on critical machinery has the potential to significantly optimize maintenance procedures and reduce waste, because of this predictive maintenance and CM will continue to become more prevalent now and in the future.

Chapter 3 - Experimental Setup

In order to gather data for vibration analysis, practical experiments are conducted. The setup includes experiments with both healthy and faulty bearings, however only the experiments with healthy bearings can be carried out. Nevertheless, the topic of creating faulty bearings and testing with faulty bearings is still described in the setup.

The experiments are done using an Alva X60 electric motor. The motor contains two ball bearings that will be the components of interest. The purpose of the experiments is to observe if and how vibration readings change based on the condition of the motor and bearings. Ideally, the results will showcase a clear distinction between the different setups, however what is most important is to determine how large of a distinction different setups exhibit. This will help determine the impact of each variable on the vibration levels.

There are four primary setups. These are composed by either static or dynamic movement and healthy or faulty bearings. Possible setups are:

1. **Static movement + healthy bearing**
2. **Static movement + faulty bearing**
3. **Dynamic movement + healthy bearing**
4. **Dynamic movement + faulty bearing**

(Only experimental setups 1 and 3 will be carried out for this thesis.)

With a static setup the motor is only subjected to self-inflicted vibrations and forces. With a dynamic setup, the motor is additionally subjected to dynamic flight forces. As such, the dynamic experiments will be more comprehensive, however it also has more variables to consider. The static setup should be carried out first to consider the results with fewer variables. With fewer initial variables it will be easier to identify and work out any potential problems or surprises.

3.1 Experimental design

In order to compare results, different test setups need to be considered. The different setups are designed to explore as many variables and factors that affect the vibration as possible. The baseline frequency is the motor being run with healthy bearings. Another element is added with the dynamic setup, but a baseline dynamic range with healthy bearings can also be determined. Moving from this baseline, some level of failure can be applied to explore possible vibration changes. Starting with a severe failure case is helpful for determining whether bearing vibration changes can be noticeable in the worst-case scenario. If this difference can be clearly established, it would then be practical to start looking at less severe failure cases as well.

When performing the experiments, the motor should be run at high RPM. This serves the function of exposing the motor to stress while also accelerating the testing. With a higher RPM, potential vibration patterns caused by faulty bearings could become apparent faster or more frequently. When combining this with dynamic movement as well, the failure patterns may become even more apparent. Combining drastic dynamic movements, faulty bearings, and a high RPM all together at the same time provides a good environment for fault induced vibrations to appear.

3.1.1 Experiment process

To perform the experiment the following is needed:

- Electric motor
- Healthy and faulty bearings
- Motor rig
- Vibration sensor
- Data-gathering system

The sensor should be placed on the motor, as close as possible to the bearings. The motor needs to have the correct bearings installed , either through having 2 motors, one with healthy and one with faulty bearings, or by changing the bearings as needed in one motor. With the sensor and bearings installed, the motor can be installed onto the rig. The sensor also needs to be connected to the data gathering system so that the data can be logged while the motor runs. The experiment can then be conducted. The data gathering frequency depends on the length of testing. The data is gathered from each setup and the different setups may be compared through data processing.

3.2 Experiment hypothesis

A hypothesis regarding how different variables and factors could affect the experiment and the results will be established. The hypothesis is based on what is known through literature study as well as what can be considered reasonable assumptions.

The static test should produce more predictable and stable vibration readings as the system is running at a constant rpm with no outside forces. As such all the forces are generated by the rotational energy from the motor. For the dynamic test, a more chaotic vibration image is to be expected due to the motor being in movement constantly. Therefore, it will be harder to identify which vibration readings could possibly be linked to bearing failure. By doing the static vibration analysis, the expectation is that a clear difference will be observed between the healthy and rusty bearings. If a difference in vibration patterns can clearly be established through the static test, that will then provide a guide of what to look for in the dynamic test as well. If only the dynamic test were to be carried out, then it might be difficult to know what to look for in the vibration data.

One of the failure mode options is rusty bearings. By using this option the bearing surface friction should also increase. With the motor also running at a high rpm the motor will on average be subjected to larger forces than it would through normal operating conditions. In addition, the bearing lubrication will also get tampered with during the rusting process. By running the motor in these “extreme” unfavorable circumstances, the likelihood of seeing the vibration effects of the faulty bearings should increase. The bearing vibrations may also be visible when running the motor at lower RPM, but it might take longer for them to become apparent. A severely rusted bearing is perhaps a somewhat exaggerated motor fault, but it should also give a more clear or obvious result on the vibration spectrum. This is helpful given the extra noise/vibrations that will appear from the dynamic movement testing. Alternatively, a scratched bearing could be used, and while that may have less of a vibration impact, it also reduces the likelihood of damaging the motor as there isn’t a risk of rust spreading around the motor.

As the testing begins, the bearing is already subjected to a severe fault which is likely generated through means that are faster than naturally occurring failure. The tradeoff with accelerated testing is that the fault doesn't develop naturally over time, as such the initial vibration patterns might not match up with the expected pattern from any of the 4 failure stages (Figure 8). It might take some time for defects to appear on the bearings, as the bearing needs several rotations before the rust starts to chip away at the bearing surfaces. It's possible that the initial vibrations will match the signature stage 1 or 2 vibration patterns, but it is unclear whether this will be the case. However, after running the motor for a period, the vibration pattern should eventually start to fit into one of the 4 failure stage patterns. Due to the severity of the failure, a reasonable assumption is that once the patterns starts to match up with one of the failure stages, it will be one of the later ones, that is stage 3 or 4. However, if the vibrations only match up with stage 4 due to severity of the fault, it might be hard to actually match them up due to the prevalence of random vibrations in stage 4. Because of this, trying to find a pattern that matches the standard fault progression may be futile. If this is the case, then the signs to look for in the vibration spectrum could be more focused on finding vibration spikes and outliers from the random vibrations that could indicate a fault.

By utilizing different data processing methods; FFT, RMS and PSD, more data parameters can be gathered from the vibration profile. Patterns that don't appear in a time domain analysis could for example show up in the PSD instead. In addition, looking at the frequency domain or PSD can give information regarding which frequencies are most prevalent. By utilizing all these methods, a clearer picture should emerge to help detect fault induced vibrations.

3.3 Sensor

The chosen sensor is the "830M1 TRIAXIAL CONDITION MONITORING ACCELEROMETER" (part of the datasheet is in Appendix C). This sensor was chosen because it is triaxial and it fits the size constraints in the motor. The sensor being triaxial is an advantage since it provides more information for a single test, while with a single axis sensor it might take more tests if there are multiple relevant axes to consider. As mentioned in the previous section, there are size constraints to consider, and with the sensor size at 15x15x4mm it allows for optimal placement during testing. The range of the sensor is up to 15 kHz which should cover all relevant vibration frequencies. Lastly it has a measurement range of ± 25g and a sensitivity of 50 mV/g which should be sufficient for this test since excessive double-digit g forces seem unlikely.

After the sensor data is gathered it also needs to be processed. Only having the time domain or frequency domain may not be enough to detect faults. Therefore, the data may also be processed with FFT, PSD and RMS. Processing and presenting the data with different parameters allows for the data to be interpreted through multiple angles. FFT ensures an insight into both the frequency and time domain. RMS and PSD are utilized to present the energy and power content of the vibration spectrum (PSD also shows how it changes over time).

3.3.1 Sensor placement and dimensioning

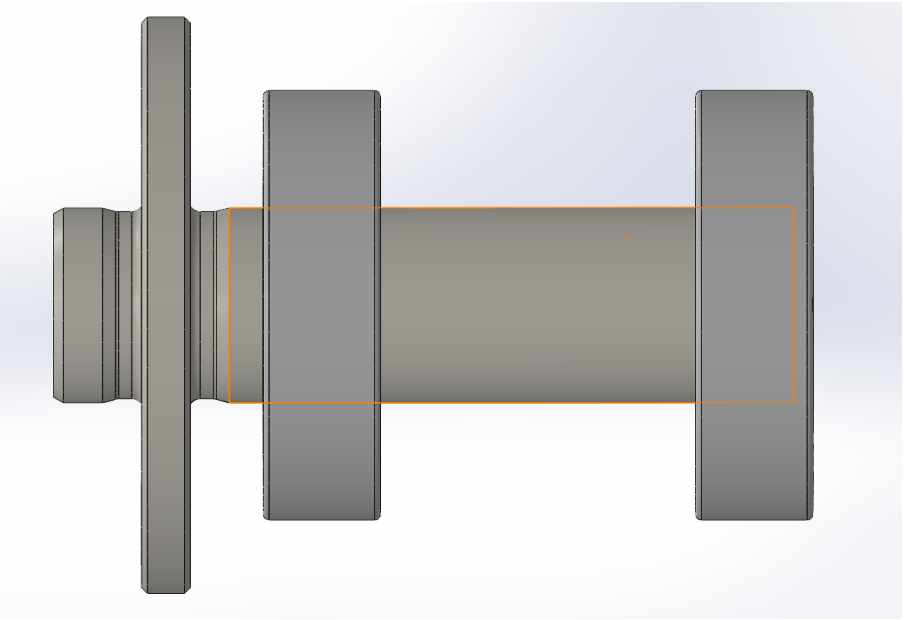

FIGURE 16 STRIPPED DOWN MOTOR. SIDEWAYS VIEW SHOWING BEARINGS AND AXLE

When it comes to sensor placement, the sensor is more likely to pick up on bearing vibrations the closer it is located to the bearing. As there are two bearings, the ideal spot would be as close as possible to both. A beneficial setup would be to place the sensor right in the middle of the two bearings. Between the edges of the two bearings there is 18mm of free space.

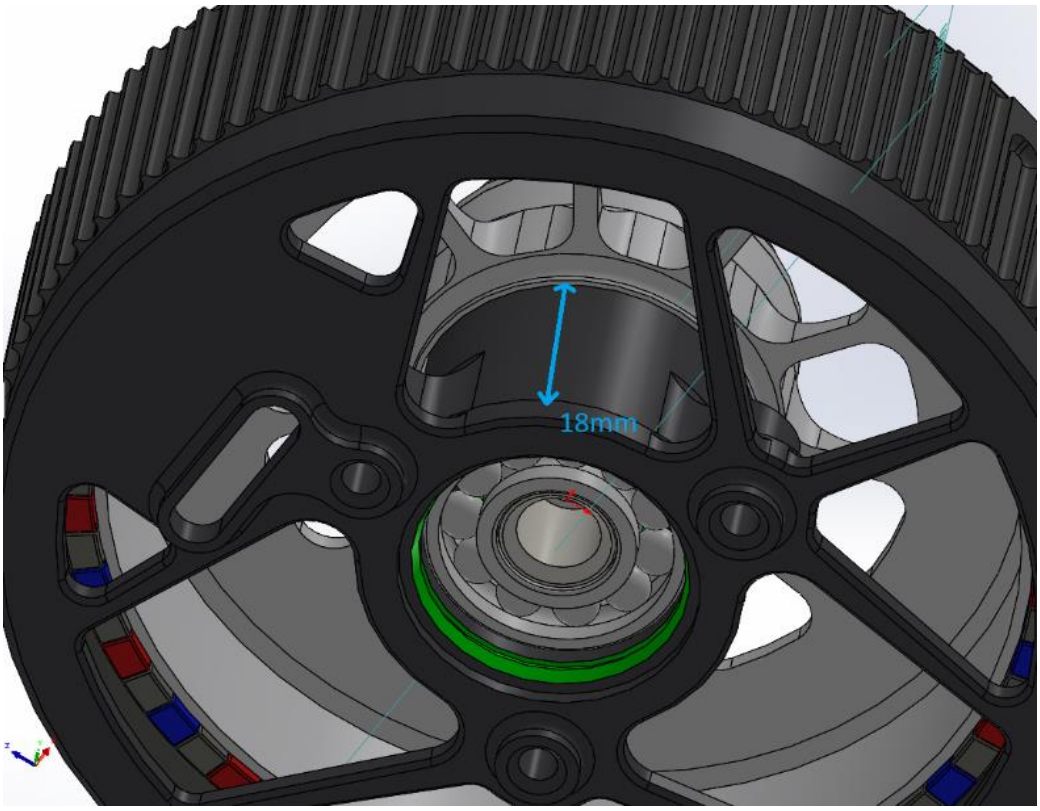

FIGURE 17 3D MODEL OF MOTOR ILLUSTRATING SPACE FOR SENSOR PLACEMENT ON THE MOTOR

Looking at Figure 17, it can be seen that the bearing can be placed on the shaft that covers the bearings. However, there are some size limitations that the sensor must fit within in. The strictest of these limitations is the space between the two bearings which is 18mm. This requires a relatively small sensor. In addition, the surface connection circular, therefore a flat surface must be added instead.

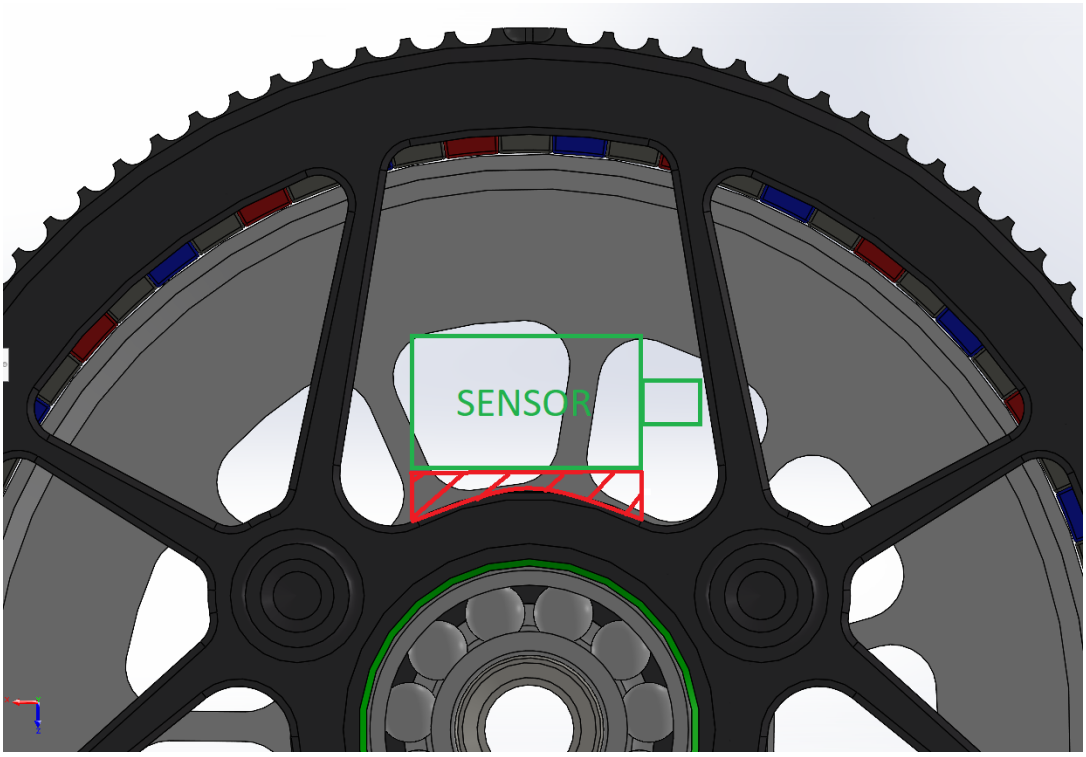

FIGURE 18 2D ILLUSTRATION OF SENSOR PLACEMENT. THE RED FIGURE IS THE SENSOR PLATFORM

In order to create a flat surface for the sensor, a custom piece is created to snugly fit over the circular surface (Figure 18). If the bottom of the piece fits on the surface, the top part can be flat which allows for the sensor to be placed properly. This piece can be 3d printed and customized to the sensor of choice. Accommodating a flat surface can be for the entire base of the sensor will allow for the best sensor performance as the vibrations will be evenly distributed to the sensor.

Alternatively, the sensor may be placed on or inside the motor hub. This is worse than placing it as close as possible to the bearings as the sensor will be more prone to pick up other vibration sources than the bearings. On the other hand, it could be a better placement because it is likely more realistic to a real-life scenario. In a real drone CM scenario, it is likely more viable to have the sensor in the hub because it is easier to make space there and the sensor won't potentially interfere with the motor performance. While it might be harder to pickup and isolate the vibration contributions from the bearings this way, it should still be possible to gather valuable data.

3.4 Failure modes

There are several failure modes the bearings can be exposed to. Some of the most practical and viable failure mode options for the experiment will be presented in this section. One of these is physical damage on the bearings. This could be something like the failure described in chapter 2.4.3 (Figure 15) which consists of a machined hole on the roller element(s). This fault produces a clear effect on the vibration spectrum, as showcased in the aforementioned chapter. It is also one of the faults that is likely to occur naturally through use of the motor, which makes it a realistic and impactful failure mode to apply. However, physical bearing damage can manifest in many different ways, and there might be significant variance in the way each way impacts the vibrations. There are also different magnitudes to consider as smaller damages will likely have less of an effect than something like large scratches or chips. As such, what type of damage to inflict on the bearings should be considered carefully.

Another option is to use an already worn-out motor. The bearings on the motor could for example be damaged from wear caused several hours of motor usage or if the motor has undergone accelerated or stress testing. This is a practical option that will likely present a realistic fault, however it could be hard to reproduce the resulting faults based on which method was used to generate it.

Exposing the bearings to rust could be another option. Rust is an impactful problem for the health and performance of a bearing. By using rusty bearings in the motor, it is put through conditions that are perhaps tougher than what is expected in a real-life scenario. This is however beneficial to the experiment as it might make it easier to determine whether the bearing vibrations can be singled out in a noisy environment. In addition, rust is easier to induce in a consistent manner. If each bearing is treated to become rusty in a similar method and timeframe, then each bearing should have a similar level of rust and failure potential. This reduces the impact of variance for the different bearings used in the experiment. The process of rusting the bearings is done by submerging them in vinegar for a set period (acid bath). After sitting in the vinegar, the bearings are exposed to air and begin to rust.

3.4.1 Rusting method

When testing faulty bearings, the bearing fault needs to be reproducible and consistent to ensure quality testing. If the bearings are faulty in a different way every time a new test is conducted, the results may not be consistent or reproducible. The method to achieve consistently rusted bearings is done by submerging them in vinegar and drying them until the desired level of rust is achieved.

FIGURE 19 BEARINGS SUBMERGED IN VINEGAR

The bearings are place in a plastic container with 7% vinegar. The bearings are submerged in the vinegar. After they are covered, then can be removed and dried.

FIGURE 20 VINERGAR COVERED BEARINGS SET TO DRY

It takes about 20 minutes for the bearings to dry. While they dry, the acid in the vinegar along with oxygen in the air starts to corrode the bearing surfaces.

FIGURE 21 RESULTING RUSTED BEARINGS

After repeating this process several times the bearings starts to become rusty. The lubrication is also affected through this process. (IMS)

Chapter 4 - Results

Experimental work was carried out to measure vibrations from an X60 motor. Following the complete setup described in “Chapter 3 – Experimental Setup” was attempted, however due to certain time and resource constraints, some compromises had to be made. Instead of doing the experiment with faulty and healthy bearings, it was only done with healthy bearings. It was not possible to acquire a worn out or faulty motor and it wasn’t possible to switch out the healthy bearings for faulty ones either, which made it hard to implement any of the bearing failure modes. As the experiment with faulty bearings could not be carried out, alternative vibration data was used as well. This alternate data consists of two datasets of a rotating bearing, one with a healthy bearing and one with a faulty bearing.

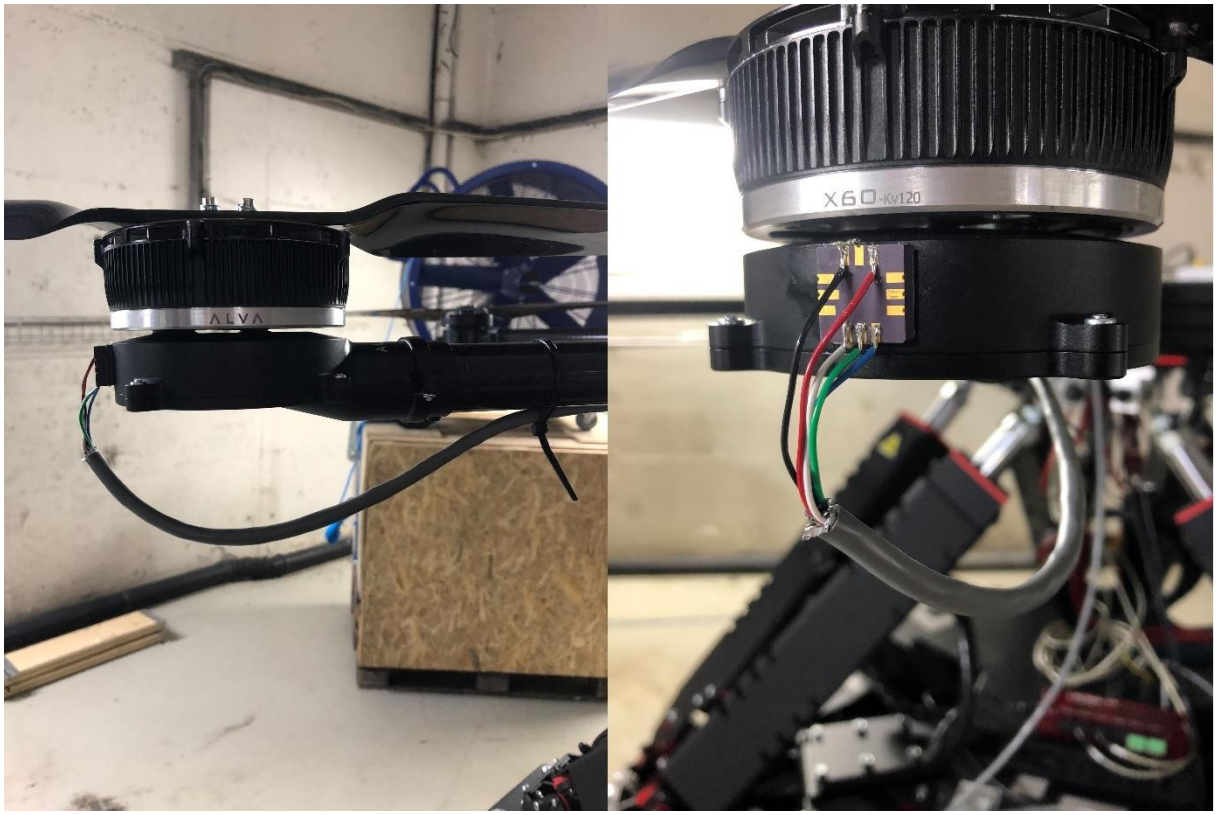

FIGURE 22 TEST SETUP. LEFT SHOWS THE MOTOR PLACED ON THE END OF AN ARM ATTACHED TO THE DYNAMIC MOVEMENT RIG. RIGHT SHOWS THE SENSOR (830M1).

As shown in Figure 22, the motor is placed on the movement rig with a propeller and a hub underneath. The sensor is placed on the hub rather than the motor. This was done to make the tests more practical to prepare and execute. As previously mentioned, this placement has its pros and cons. The advantage with this placement is that it is more realistic with regards to a real-world scenario, as it is closer to where the vibration sensor would actually be placed if it were to be integrated as a permanent part of Alva’s motor design. The main disadvantage is that it is placed farther away from the bearings, which might make it harder to pick up their vibrations.

4.1 Static and dynamic healthy bearing data analysis

The testing was done with the setup described in the previous section. Two different setups are used for testing. One is the static test, where the motor is running without any movement from

the dynamic rig. The other is the dynamic test, where the motor and rig are running simultaneously to expose the motor to dynamic forces. The motor ran at about 3500RPM for each test. The sensor data was sampled at 30kHz, and each recording is 1 second, giving 30000 data points for each recording. The raw sensor data (which is in the form of voltage) for both the static and dynamic tests were subtracted by a baseline recording, using the same parameters done with the sensor at zero movement or vibration (except any potential background noise). The subtracted data was then converted from voltage values to to amplitude (g) values, which describe the forces subjected to each sensor axis. The data was then processed through Matlab code (Appendix A) to provide time domain, frequency domain and PSD graphs for each axis (Figure 23). FFT was used since the recording times are quite low and because PSD is utilized as well, which ignores bin width(how wide the analyzed slices of time are) and already shows how the frequencies change over time. This would make the used of STFT somewhat redundant.

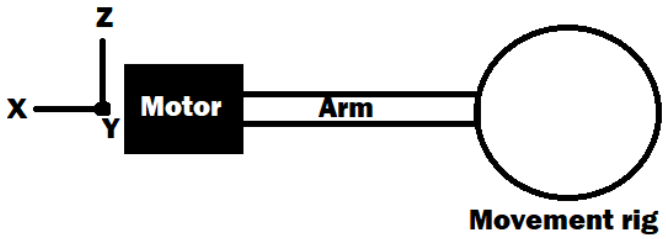

FIGURE 23 TOP-DOWN VIEW OF TEST-SETUP ILLUSTRATING WHICH DIRECTION EACH SENSOR AXIS REPRESENTS

The x-axis will primarily be analyzed because it is the axis that showed the largest effect from the introduction of dynamic conditions. Because of this, it provides the best example for analysis. The complete data for the y and z axes can be found in Appendix B. The data for all the axes show the most relevant frequencies to be at 0-2000Hz, with the z-axis also having some frequency spikes up to and around 10000Hz as well. With the motor running at 3500rpm, the rotational frequency of the motor should be about 60Hz and a small spike at 60hz in every axis' frequency domain graph can be observed as well.

Looking at the vibration data from the different axes there are some differences to the way they react to the dynamic conditions. The y-axis doesn't show a big change from static to dynamic movement. The dynamic data shows that the time domain gets slightly more chaotic and the prevalence of some frequencies change, however the difference is not very large.

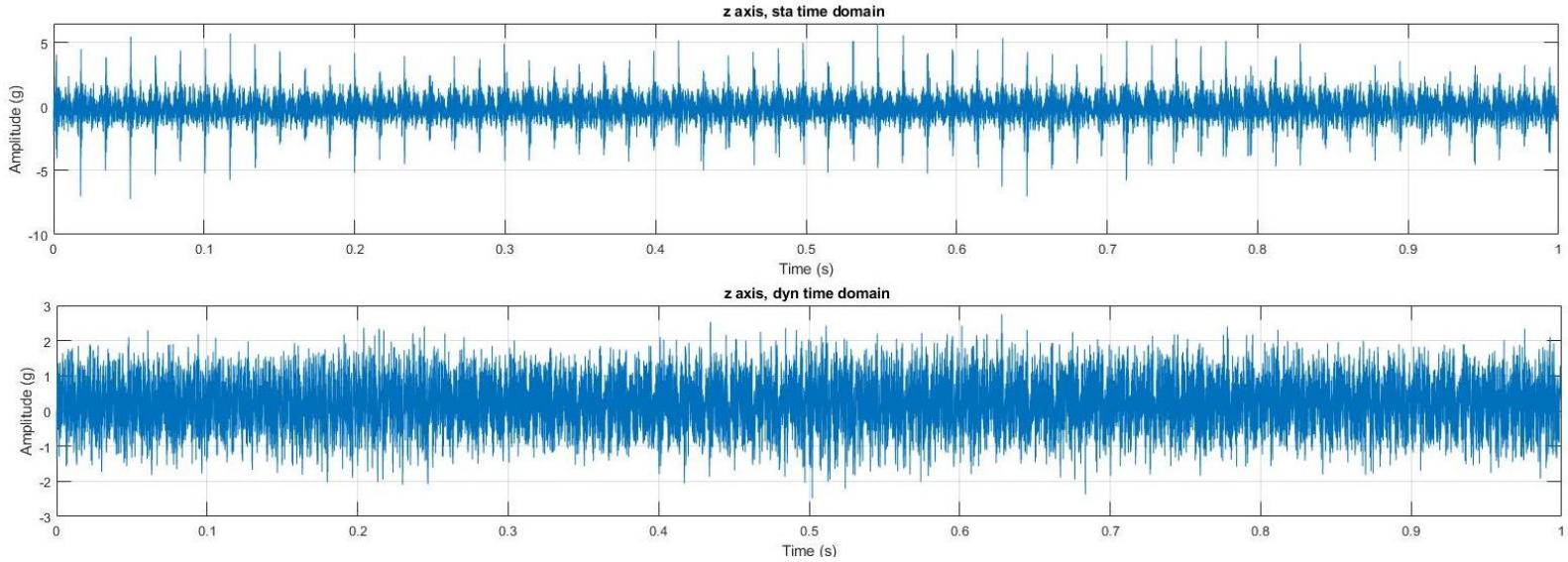

FIGURE 24 COMPARISON OF STATIC AND DYNAMIC TIME DOMAIN VIBRATION DATA FOR THE Z-AXIS

Looking at the z-axis amplitude spikes in the $3-5g$ range consistently appear in the static data, however in the dynamic data spikes of this magnitude are absent. However, the PSD still shows the distributed power levels of the frequencies to be similar.

Table 3: RMS values of the amplitude (g) for each axis

	X	Y	Z
Static experiment	0.075	1.8819	0.8878
Dynamic experiment	1.345	1.6294	0.6960

Looking at the RMS values for each axis, the x-axis value shows a drastic increase from static to dynamic movement. On the other hand, the y and z axes show a minor decrease in RMS values from static to dynamic movement. Overall, the RMS is higher for the dynamic case, but all of this increase is concentrated on the x-axis.

4.1.1 Static and dynamic data of the x-axis

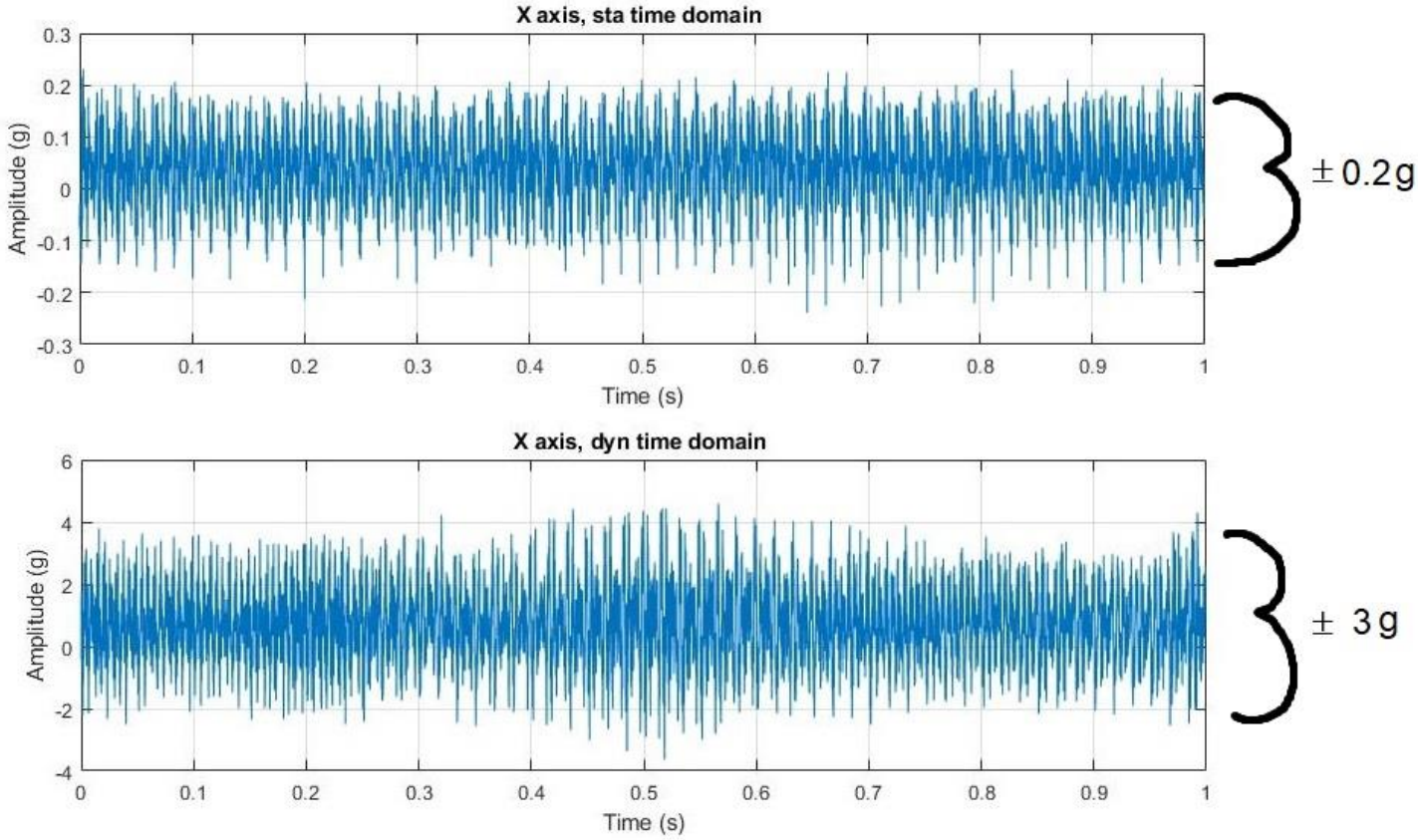

FIGURE 25 COMPARISON OF STATIC AND DYNAMIC TIME DOMAIN VIBRATION DATA FOR THE X-AXIS

Looking at the time domain for the x-axis (Figure 25), there is a similar distribution pattern between the static and dynamic graph. The big difference is that the amplitude is exaggerated for the dynamic case, with the highest peaks around 20 times higher than the static peaks.

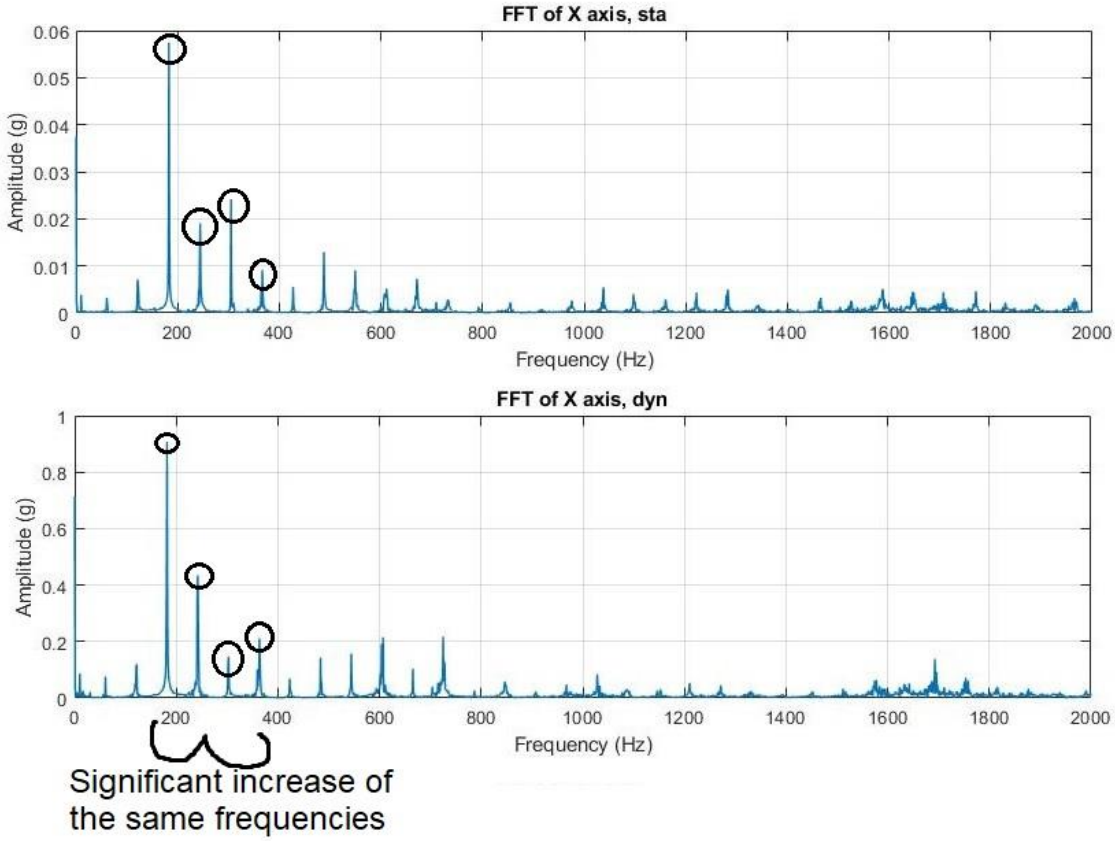

FIGURE 26 COMPARISON OF STATIC AND DYNAMIC FREQUENCY DOMAIN VIBRATION DATA FOR THE X-AXIS

Looking at the frequency domain, four example frequencies (at about 180, 240, 320 and 380 Hz) are shown in Figure 26 that illustrates the similarities and differences between the two graphs. Most of the same frequencies are prevalent in both the static and dynamic graphs, however a significant increase in some frequencies are apparent in the dynamic graph, with the differences getting up to around 20-fold.

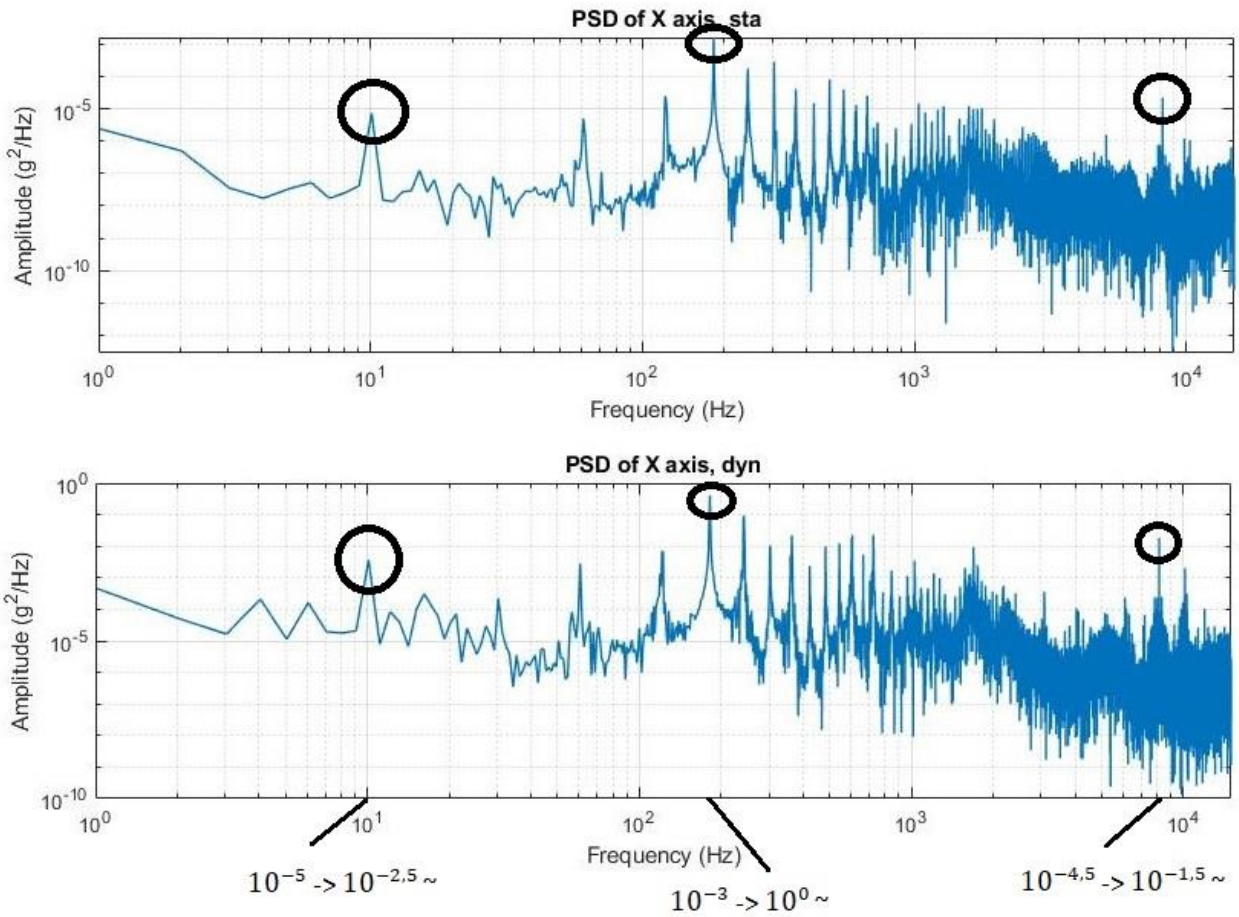

FIGURE 27 COMPARISON OF STATIC AND DYNAMIC PSD VIBRATION DATA FROM THE X-AXIS

Comparing the PSD graphs, the patterns present in the two graphs are very similar, but with the power distribution being higher on the dynamic spectrum. This is illustrated on Figure 27 where 3 data points (at about 10, 190 and 9000Hz) show a similar increase of around $10^3\ g^2/Hz$.

4.2 Alternative data analysis

This dataset is from Mendeley Data (Huan Huang & Baddour, 2018) and contains vibration data from different bearings at different health conditions undergoing varying rotational speed. The data is sampled by an accelerometer at 200kHz and lasts for 10 seconds. There are two datasets of choice, the first is H-C-1, which is a healthy bearing which first rotates at 14.7 Hz to 25.3 Hz and then decreases to 21.0 Hz. The second is I-C-1 which is a bearing with an inner race fault which first rotates from 15.1 Hz to 24.4 Hz and then decreases to 18.7 Hz.

4.2.1 Healthy bearing data H-C-1

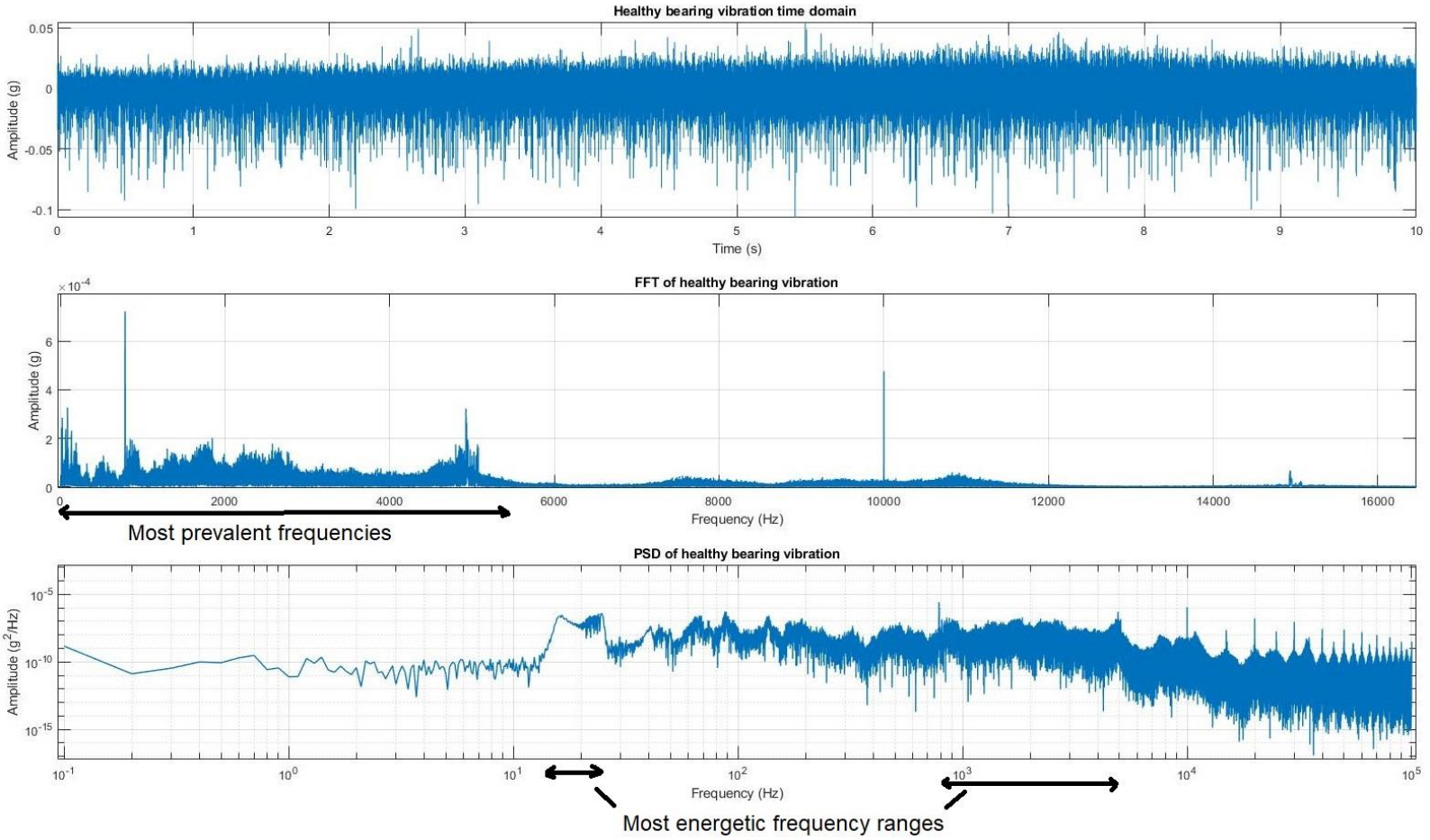

FIGURE 28 TIME DOMAIN, FREQUENCY DOMAIN AND PSD(LOG SCALE) OF HEALTHY BEARING VIBRATION DATA

The time domain graph shows that the vibrations consistently fluctuate between $\pm 0.05g$, with peaks at $0.1g$. Differences in rotational speed through the 10 seconds are not very visible by looking at the time domain. The frequency domain shows the dominant frequencies to be between about 10-5500Hz with spikes at around 1000, 5000 and 10000 Hz. In the PSD, spikes at around 1000 and 5000Hz are also visible and it illustrates the strongest energy content in the 20-4500Hz range.

4.2.2 Inner fault bearing data I-C-1

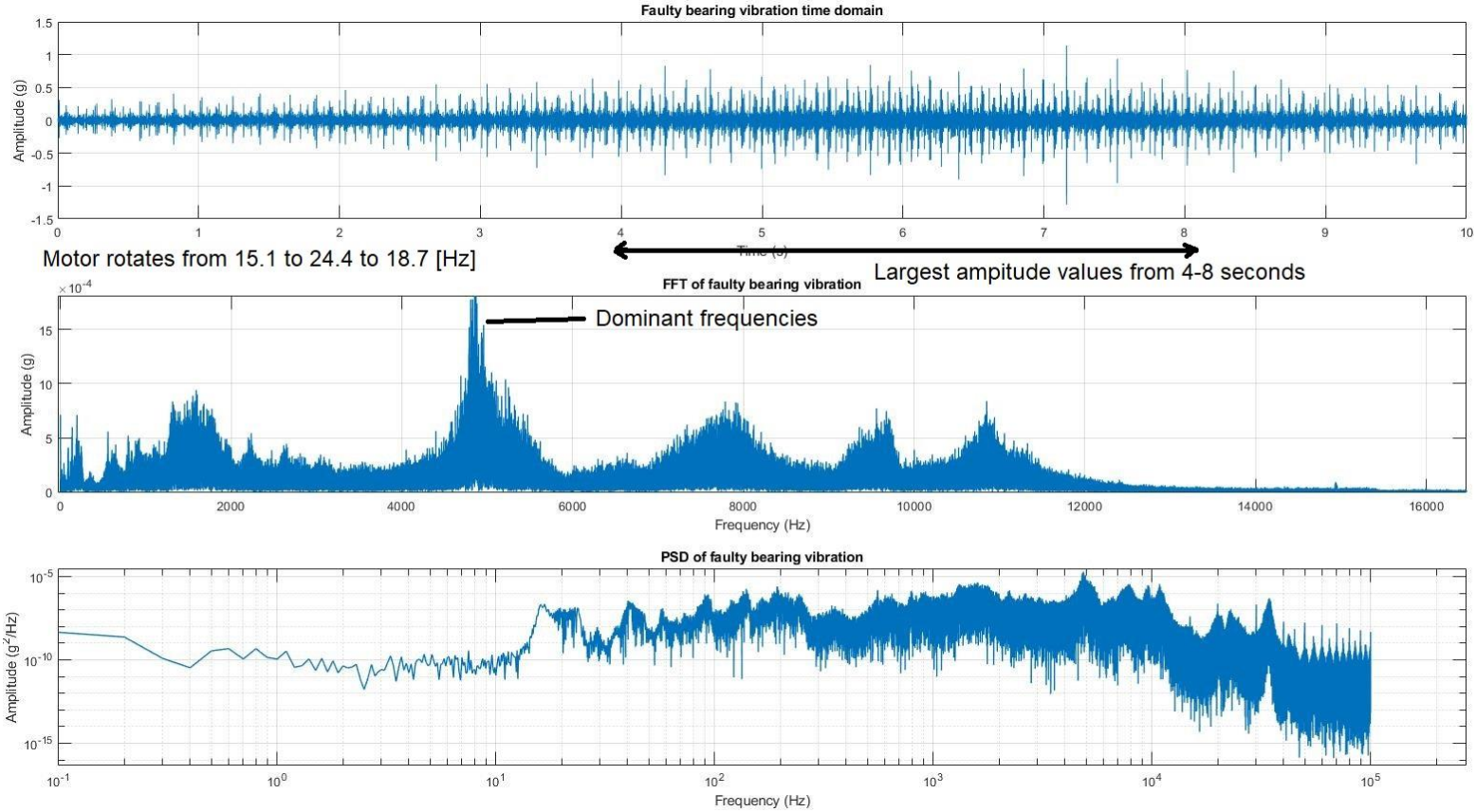

FIGURE 29 TIME DOMAIN, FREQUENCY DOMAIN AND PSD(LOG SCALE) OF FAULTY BEARING VIBRATION DATA

The time domain graph for the faulty bearing shows a constant fluctuation between ± 0.5, however the rotational speed differences can be seen with the fluctuations at their lowest in the first 3 seconds and at their highest between 4-8 seconds. This matches the experimental setup which describes bearings starting at 15.1 Hz, then speeding up to 24.4 Hz, and then decreases to 18.7 Hz. The FFT illustrates a dominant frequency around 5000Hz as well. The PSD shows similar tops around 4000-6000Hz.

4.2.3 Comparison between healthy and faulty bearing data

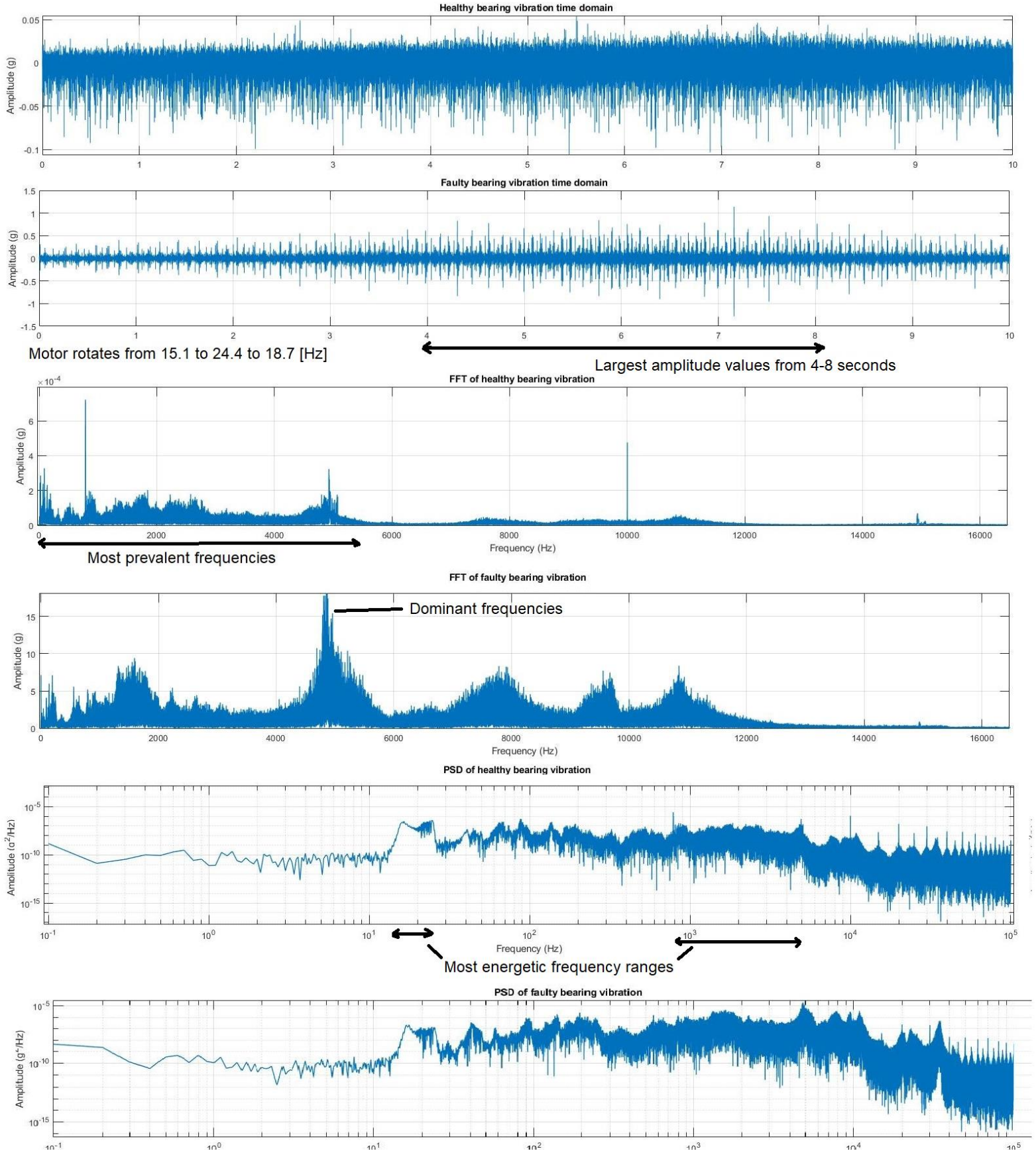

FIGURE 30 COMPARISON OF TIME DOMAIN, FREQUENCY DOMAIN AND PSD OF HEALTHY AND FAULTY VIBRATION DATA

Comparing the healthy data with the faulty data, a clear distinction can be seen. Though both the healthy and faulty graphs follow a similar pattern in the frequency domain and PSD, the amplitudes are higher in the faulty case. Comparing both the time domain and frequency domain graphs shows that the faulty bearing vibrations exhibit higher amplitude levels throughout the 10 second period and across several frequencies. Some of the amplitude spikes are around 10 times as high as the ones from the healthy vibration graph. The prevalence of frequencies around 5000Hz increased about 7-fold. The PSD graph illustrates a similar power distribution pattern in both graphs; however, the faulty PSD shows a general higher level of energy content throughout the different frequencies. Increased energy levels from the faulty bearing vibrations as also visible in the RMS values (Table 4).

Table 4: RMS values of the amplitude (g) for each dataset

Healthy bearing	0.0083
Faulty bearing	0.0509

4.3 Discussion

Some factors could contribute towards questioning the validity or certainty of the experimental data. For example, the sensor placement. Would having the sensor closer to the bearings create more accurate vibration data with regards to the bearing vibrations? Is 1 second of data sufficient to have a comprehensive overview? Was there too much background noise? Did the sensor function properly during testing? Determining the magnitude of such factors on the data could be beneficial to any future experiments with a similar setup to the one conducted at Alva.

Another important point to consider is how well the dynamic rig manages to emulate drone movement and forces. Though it is clear that the dynamic movement from the rig makes an impact on the vibration levels, does it match the vibrations that would be produced by a real drone in flight? An example of a difference between the two is that unlike a drone, the movement rig is limited to how long and far it can move the motor in one direction as the range of movement is a lot more limited. Additionally, when looking at the distribution of the vibration energy content through the RMS values(Table 3) it seems that most of the vibration energy is transferred towards the x-axis, as it has a large increase in RMS value from static to dynamic movement, while y and z lose some energy from static to dynamic movement. Because of this, it might be prudent to, in the future, do experimental work with a real drone in flight to see how the data from the dynamic rig measures in relation to a real drone.

Looking at the alternative data, a clear distinction is visible between the healthy and faulty bearing data. All metrics of amplitude, energy content and frequencies show an increase for the faulty bearing, and this is most apparent with the amplitude where the faulty data could spike at peaks more than about 10 times the healthy data. The frequency pattern of the faulty frequency domain graph is similar to the healthy graph, but with a significant increase of the prevalent frequencies. A possible explanation for this observation is the possibility that the increase in vibrations occurring from the faulty bearings is causing resonance that amplifies the system's natural frequencies.

Similarly to the comparison between the healthy and faulty bearing data, the comparison between the static and dynamic data for the x-axis showed similar patterns. The dynamic time domain showed an increase in amplitude many times that of the static data. Looking at the frequency domain, there is also a large increase in the prevalence of the same frequencies from static to dynamic, which again could be attributed to resonance. The PSD also has a similar trend between the static and dynamic data, with some of the data points having been directly compared showing a consistent increase in power levels from static to dynamic readings.

A similar effect has been illustrated from introducing a faulty bearing to a motor and from introducing dynamic conditions (at least in one axis). Considering this, can one conclude whether the vibrations from the faulty bearing are visible through the vibration noise introduced by dynamic movement? That is difficult to definitively conclude as there are two different experimental setups to consider with different parameters. It might for example not be very helpful to compare amplitude levels between the two experiments as they run with different setups with different RPM, motors, bearings etc. However, both the alternate healthy/faulty data and the static/dynamic x-axis data showed signs of resonance and it can be speculated as to whether the increase in resonance coming from the faulty and dynamic conditions would overlap to create even more chaotic/random or exaggerated amplitude values. If this is the case, then it suggests that a difference could be discerned between a healthy motor in dynamic

conditions and a faulty motor in dynamic conditions (at least in the time domain), even through the noise of the dynamic conditions. Additionally, it is worth considering that each axis x, y, and z reacted somewhat differently to the dynamic conditions. While this difference might be nothing more than the magnitude of the dynamic forces being lower/higher in different axes, it is worth keeping in mind that there is additional information to be gained in analyzing multiple axes. For example, if there happened to be certain vibration spikes indicating a bearing fault, those could be visible in the z-axis and not in the x-axis. Whether different axes would respond differently to faulty bearing vibrations the same way they did dynamic movement vibrations, is something that can be discovered through future experimental work.

To gain a more definitive answer to the research question and accompanying questions/unknowns, an experiment should be conducted that combines the different factors all at once, comparing motors with healthy and faulty bearings in static and dynamic conditions. Nevertheless, the information gained from the experimental work and analysis provides insight into the effects of bearing vibration and it indicates that there is validity to the idea of using vibration analysis as a condition monitoring tool for drone motors.

Chapter 5 - Conclusion

The purpose of this thesis was to investigate whether vibration monitoring could be utilized to detect electric motor issues in drones. The motor bearings were chosen as the component of interest, as they are the primary source of motor faults in electric motors. To help answer the research question, a review of relevant theory was conducted. In addition, an experiment was designed to gather data that would provide information towards answering the research question.

The experiment was carried out using a triaxial accelerometer attached to an electric motor with healthy bearings set up on a dynamic motion rig that mimics drone movement. Data from this experiment was analyzed by looking at and comparing the vibration from the motor running with no movement (static) as well as with the dynamic rig in movement (dynamic). Additionally, alternate vibration data gathered from another experiment utilizing healthy and damaged bearings was processed and analyzed by comparing the vibrations levels of the healthy and damaged bearings.

By analyzing the vibration data from both the experiment and the alternate data, it was found that the introduction of bearing fault and dynamic conditions both had a significant effect on the vibration readings. This effect came in the form of higher amplitudes, increased prevalence of several frequencies and increased power density. However, the experiment with dynamic conditions did not demonstrate the same trend in all axes, as some axes were more affected by the conditions than others. Though it is difficult to determine whether the effects of the faulty bearing could be visible through the vibration noise created by dynamic movement, it can be theorized that some factors would make it possible. Some of these factors are the magnitude of potential resonance, the prevalence of vibration spikes/outliers, and if any of the axes show significant changes in vibration, frequency or power density.

Based on the results, there is merit to the idea that vibration analysis is viable for determining bearing faults in drone motors. Analyzing the vibration data provided several useful data points that give an impression regarding the state of the system. Based on the results there is an indication that there is value in continuing the work to decisively determine whether it is possible and practical to use vibration readings from drone motor structures to identify bearing issues.

5.1 Future work

An important continuation of the experimental work for the future lies in testing with faulty bearings. Utilizing and comparing motors with both healthy and faulty bearings for vibration testing, will clarify a lot of the uncertainties regarding the current hypothesis/theory. These experiments would help determine whether it is practically possible to determine whether the bearings are faulty through vibrations analysis alone.

Another point of interest is to test with real drones to account for possible shortcomings of the dynamic movement rig. There is theory backing up the idea that the movement rig can mimic real drone movement, but the best way to confirm whether it does a good job of recreating these movements, is to test it directly. If similar experiments with healthy and faulty bearings can be reproduced on an actual drone in motion, then that would confirm the viability of the experiments done on the movement rig.

References

Arar, S. (2022). Understanding Piezoelectric Accelerometer Basics. https://www.allaboutcircuits.com/technical-articles/introduction-to-piezoelectric-accelerometers-piezoelectric-sensor-basics/

Bartfield, R. R. S. T. G. H. F. K. R. G. (1995). Motor bearing damage detection using stator current monitoring. *IEEE*. https://ieeexplore.ieee.org/document/475697

Collins, D. (2019). How are fast Fourier transforms used in vibration analysis? https://www.motioncontroltips.com/how-are-fast-fourier-transforms-used-in-vibration-analysis/

Dai, S. A. M. Y. (2003). Basic vibration signal processing for bearing fault detection. https://ieeexplore.ieee.org/abstract/document/1183679

Eklund, N. (2022). Predictive Maintenance is the Future – But Not Quite in the Way You Think. https://oilmanmagazine.com/article/predictive-maintenance-is-the-future-but-not-quite-in-the-way-you-think/

electric, D. Electric Motor Failure. https://www.dukeelectric.com/electric-motor-failure/

Electric, G. I. AC and DC Motors: Differences and Advantages | Types of Electric Motors. *Gainesville Industrial*. https://www.gainesvilleindustrial.com/blog/ac-dc-motors/

Enrico Petritoli, F. L., Lorenzo Ciani. (2018). Reliability and Maintenance Analysis of Unmanned Aerial Vehicles. https://www.ncbi.nlm.nih.gov/pmc/articles/PMC6165073/#:~:text=The%20commercial%20aviation%20failure%20rate,overall%20failure%20rate%20of%2025%25.

ESEA. (2019). Failures in Three-Phase Stator Windings. https://easa.com/resources/failures-in-three-phase-stator-windings

Fant, S. (2021). Predictive maintenance is a key to saving future resources. https://www.greenbiz.com/article/predictive-maintenance-key-saving-future-resources

Feuchter, M. (2021). EFFICIENT SIMULATION OF LARGE ROLLING BEARINGS. *cadfem*. https://www.cadfem.net/en/cadfem-informs/cadfem-newsroom/video-library/video/efficient-simulation-of-large-rolling-bearings.html

Gu, Y. S. W. T. F. (2010). A simulation study of defects in a rolling element bearing using FEA. https://ieeexplore.ieee.org/document/5669813

Hanly, S. (2018). Vibration Measurements: Vibration Analysis Basics. *Endaq*. https://blog.endaq.com/vibration-measurements-vibration-analysis-basics

Homayoun Meshgin-Kelk, S. N., Seungdeog Choi, Hamid A. Toliyat. (2012). *Electric Machines: Modeling, Condition Monitoring, and Fault Diagnosis*.

Huan Huang, & Baddour, N. (2018). *Bearing Vibration Data under Time-varying Rotational Speed Conditions*. https://data.mendeley.com/datasets/v43hmbwxpm/1

IMS. How to Rust Metal. *Industrial metal supply company*. https://www.industrialmetalsupply.com/blog/how-to-rust-metal

Jagath Sri Lal Senanayaka, V. K. H., Kjell G., & Robbersmyr, J. S. L. S. S. T. K. H. V. K. K. G. (2018). Fault Detection and Classification of Permanent Magnet Synchronous Motors

in Variable Load and Speed Conditions using Order Tracking and Machine Learning. https://www.researchgate.net/publication/325838773_Fault_detection_and_classification_of_permanent_magnet_synchronous_motor_in_variable_load_and_speed_conditions_using_order_tracking_and_machine_learning

Kallaste, K. K. T. V. A. R. A. (2021). Impact of Bearing Faults on Vibration Level of BLDC Motor. *IEEE*. https://ieeexplore.ieee.org/abstract/document/9589268/authors#authors

Krishnamurthy, Y. D. X. S. M. (2011). Health monitoring, fault diagnosis and failure prognosis techniques for Brushless Permanent Magnet Machines. https://ieeexplore.ieee.org/document/6043248

LANGNAU, L. (2013). Brinelling and why bearings fail — How bearings fail Part 6 of 6. https://www.linearmotiontips.com/how-bearings-fail-a-closer-look-at-brinelling/

Liu, X. (2019). A Personalized Diagnosis Method to Detect Faults in a Bearing Based on Acceleration Sensors and an FEM Simulation Driving Support Vector Machine. https://www.mdpi.com/1424-8220/20/2/420/htm

Markets, R. a. (2022). *The Worldwide Predictive Maintenance Industry is Expected to Reach $18.6 Billion by 2027*. https://www.globenewswire.com/en/news-release/2022/04/01/2414717/28124/en/The-Worldwide-Predictive-Maintenance-Industry-is-Expected-to-Reach-18-6-Billion-by-2027.html#:~:text=The%20global%20predictive%20maintenance%20market,26.5%25%20from%202021%20to%202027.

Nicdec. https://www.nidec.com/en/technology/motor/basic/00002/

Patrick Corn, E. R., Jimin Khim. (2022). Discrete Fourier Transform. https://brilliant.org/wiki/discrete-fourier-transform/#:~:text=The%20DFT%20formula%20for%20X,%2C%20x%20N%20%E2%88%92%201%20)%20.

Reuben Lim Chi Keong, D. M. (2014). Bearing Time-to-Failure Estimation using Spectral Analysis Features. *Cranfield University*. https://core.ac.uk/download/pdf/20338922.pdf

Robbersmyr, J. S. L. S. S. T. K. H. V. K. K. G. (2017). Early detection and classification of bearing faults using support vector machine algorithm

IEEE. https://ieeexplore.ieee.org/document/7947755

Sensegrow. (2020). *What is Vibration Analysis?* https://www.sensegrow.com/blog/vibration-analysis#

STI Field Application Note. (2012). *STI Vibration monitoring*. https://www.stiweb.com/v/vspfiles/downloadables/appnotes/reb.pdf

Trout, J. Vibration Analysis Explained. *Noria Corporation*. https://www.reliableplant.com/vibration-analysis-31569

Tsypkin, M. (2017). Induction Motor Condition Monitoring: Vibration

Analysis Technique Diagnosis of Electromagnetic Anomalies *IEEE*. https://ieeexplore.ieee.org/document/8080483

Xin Zhang, C. Y., Yaofeng Liu, Pengfei Yan, Yubo Wang, Lixiao Wu1. (2020). Dynamic Modeling and Analysis of Rolling Bearing with Compound Fault on Raceway and Rolling Element. *Hindawi*. https://www.hindawi.com/journals/sv/2020/8861899/

Appendix A – Matlab code

FFT, PSD and Spectrogram

```
function [x_3D, y_3D, z_3D] = Mide_Spectrogram(datalist,fActual,nSlicesPerSecond)
%[x_3D, y_3D, z_3D] = FFT_PSD_Spectrogram(datalist,fActual,nSlicesPerSecond)
% Given a dataset this will calculate the spectrogram
%
% Inputs:
%   datalist = two column array with time in first column, data to analyze
%       in second
%   fActual = sample rate of the data in Hertz, time between each sample
%   nSlicesPerSecond = number of slices per second to break up spectrogram
%   - resolution
%
% Outputs:
%   x_3D = time for spectrogram
%   y_3D = frequency for spectrogram
%   z_3D = amplitude for spectrogram


%Compute Spectrogram
   nPts=length(datalist(:,1));
   yfft=datalist(:,2);
   nPointsPerSlice=floor(fActual / nSlicesPerSecond);
   % for very short recordings or extreme of nSlicesPerSecond,
   % nPointsPerSlice may end up being ouside a legal range for the actual
   % data series.
      if(nPointsPerSlice == 0 || nPointsPerSlice > nPts)
         disp('nPointsPerSlice cannot be achieved; slicing adjusted.');
         nPointsPerSlice = nPts/4;
      end
   % Now try to slice/reshape the column vector to (x columns of nPointsPerSlice points each)
   % in such a way that it reshapes cleanly. We'll throw away up to 1 slice of data, but we
   % avoid reshape errors.
      yfft=reshape(yfft([1:floor(length(yfft)/nPointsPerSlice)*nPointsPerSlice]),nPointsPerSlice,[]);
      [fftrows,fftcols]=size(yfft);

   % create the lone X vector to scale these all against...
      x=[0:fftrows-1];
      recordSliceTime=datalist(fftrows,1) - datalist(1,1); % again, accurately get the elapsed time of each slice
      recordSliceTime=recordSliceTime+(recordSliceTime/fftrows);
      x = x .* (1/recordSliceTime);  % normalize frequency according to sample rate and nPts

   % Apply hamming window: w(n) = 0.53836 - .46164*cos(2*pi*n/N-1)
      window=[1:fftrows];
      windowy = (0.53836 - .46164*cos((2*pi*window(:)) ./ (length(window)-1)));

   yabs=yfft;  % pre-allocate yabs with same size as yfft

   for j=[1:fftcols]
```

```
    %yfft(:,j)=fft(yfft(:,j) );                 % not windowed
    yfft(:,j)=fft(yfft(:,j) .* windowy(:));       % windowed
    %yabs(:,j)=yfft(:,j).*conj(yfft(:,j)) / length(yfft(:,j));
    yabs(:,j)=abs(yfft(:,j)) / (0.5*length(yfft(:,j)));
    yabs(1,j)=0;        % Get rid of DC component
    %yabs(2,j)=0;     % Get rid of DC component
    %yabs(3,j)=0;     % Get rid of DC component
end


% Create reasonable default values for 'points of interest'. This is
% the section of the plot we will actually show.
    nPointsOfInterest=nPointsPerSlice /2;
    startPointOfInterest=1;
    endPointOfInterest=nPointsOfInterest;

% if user entered invalid frequency values, constrain them to a range the plot actually contains
    if(startPointOfInterest < 0)
        startPointOfInterest = 0;
    end
    if(endPointOfInterest > length(x)/2)
        endPointOfInterest = length(x)/2; % do not show user aliased data
    end

% finally, actually make the plot
    x_3D = [1:fftcols] / nSlicesPerSecond;
    y_3D = x([startPointOfInterest+1:endPointOfInterest+1]);
    z_3D = yabs([startPointOfInterest+1:endPointOfInterest+1],:);
```

Appendix B – static and dynamic sensor data (y and z)

Y-axis – static

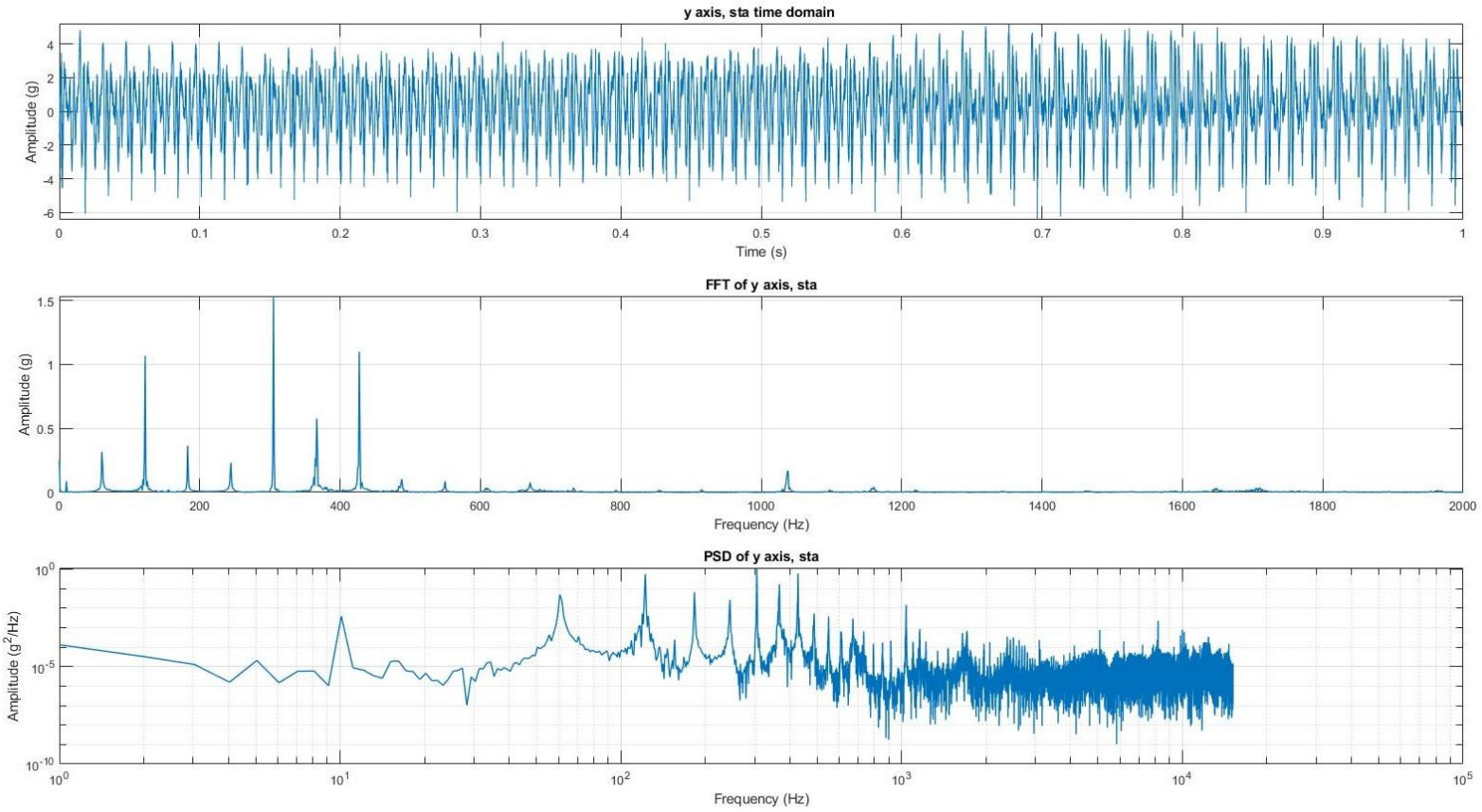

Y-axis - dynamic

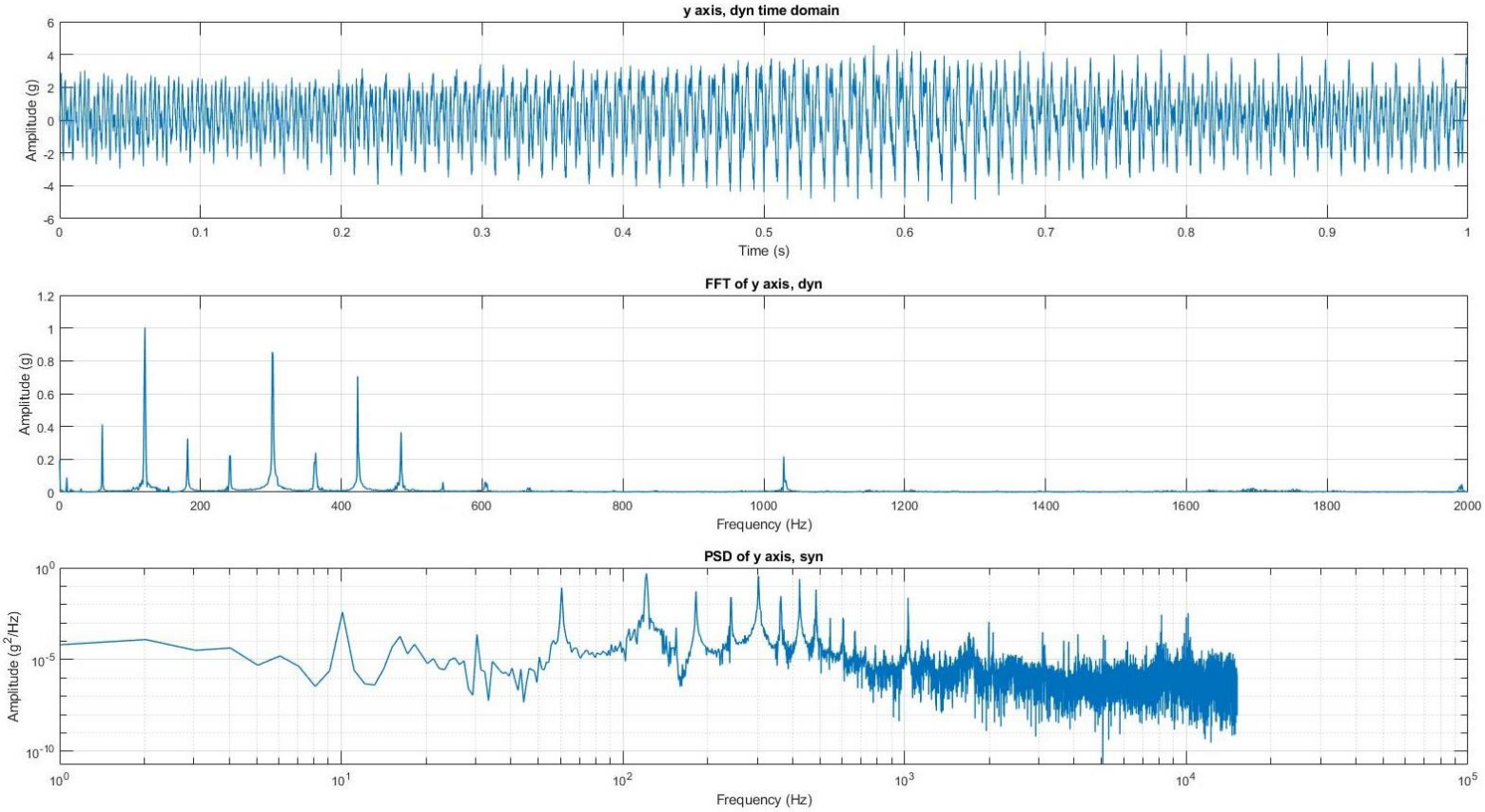

Z-axis – static

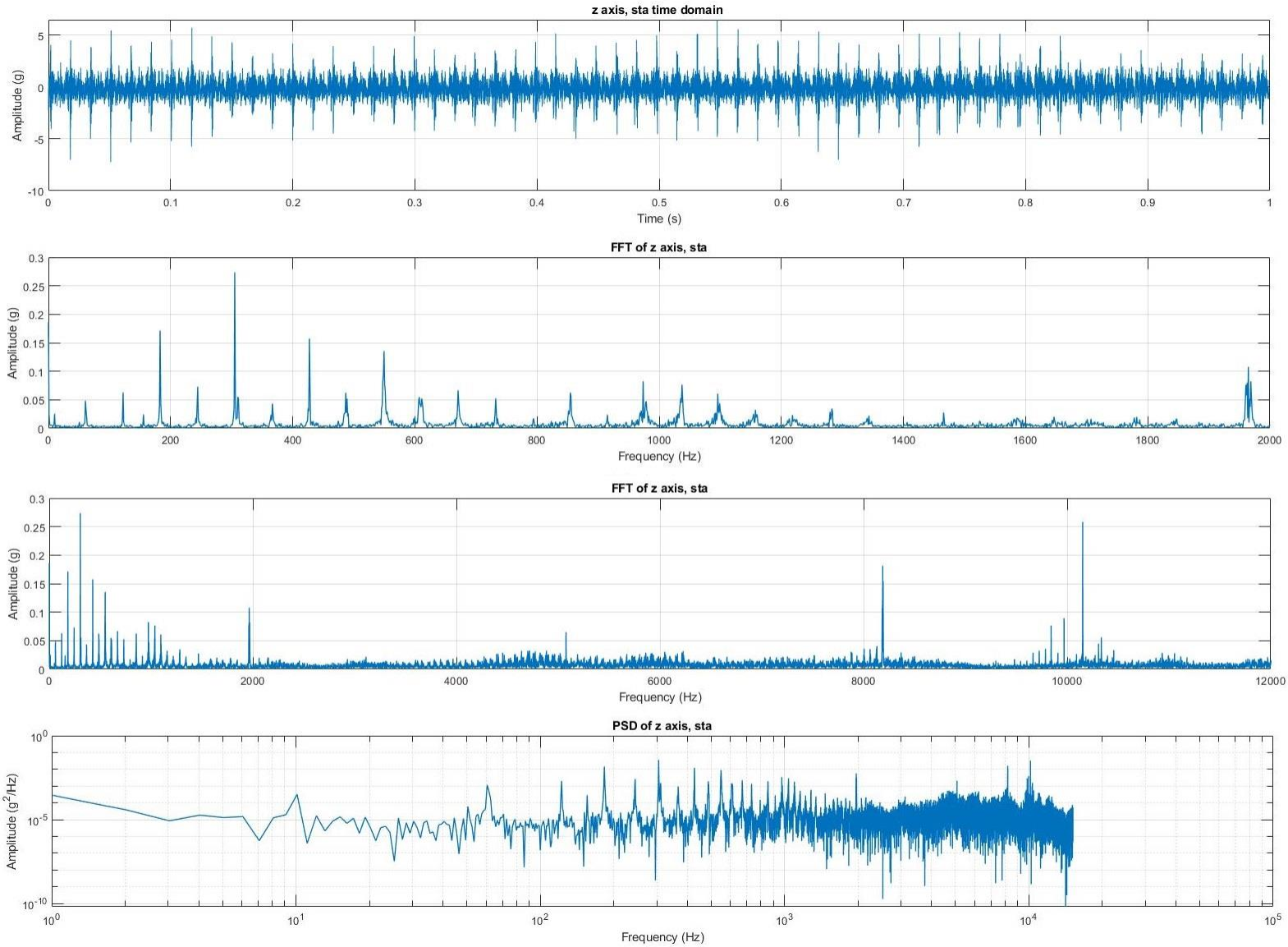

Z-axis – dynamic

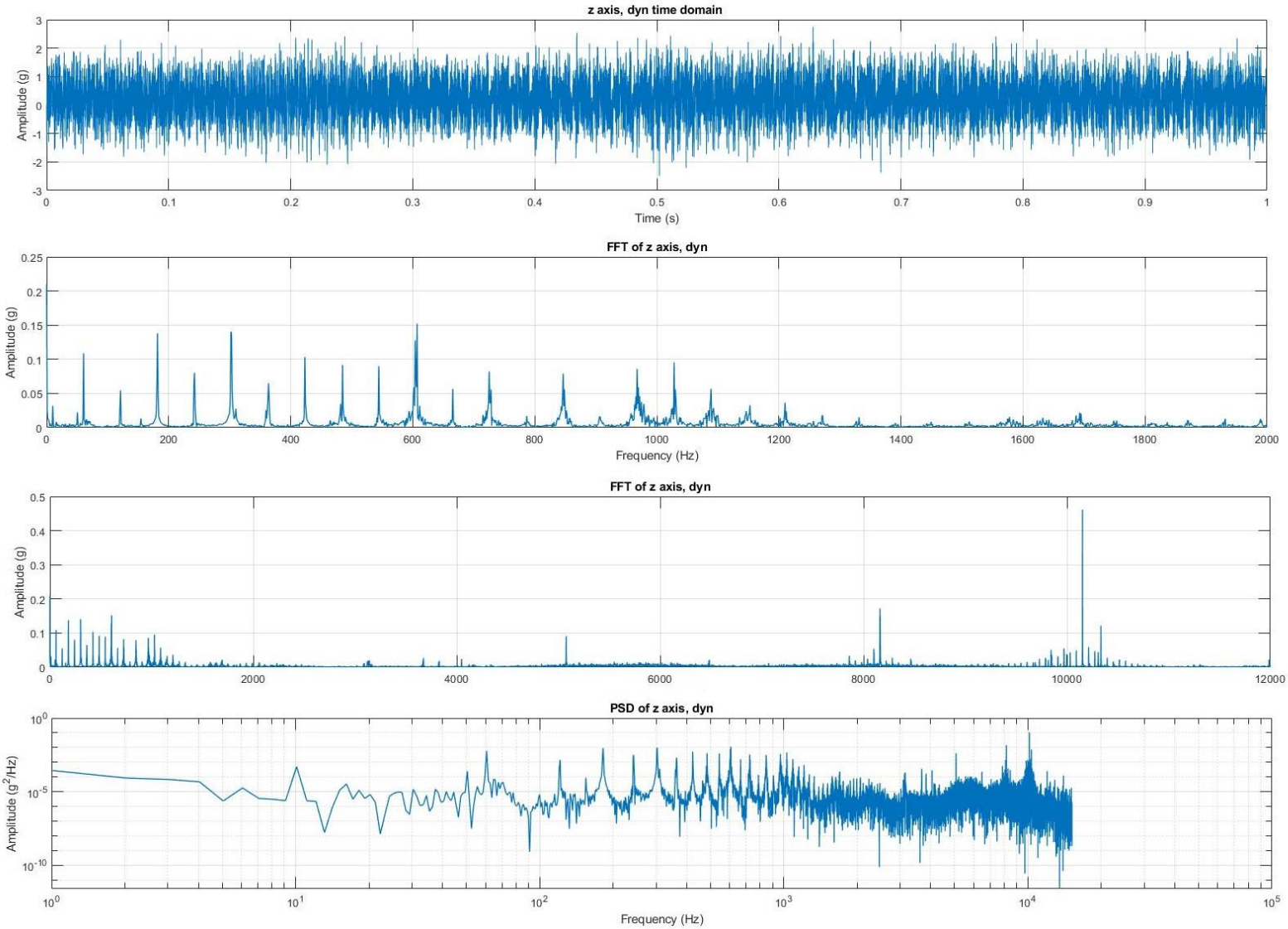

Appendix C – Sensor datasheet (pg2)

830M1 TRIAXIAL ACCELEROMETER

ABSOLUTE MAXIMUM RATINGS [1]

Parameter	Symbol	Min	Typ	Max	Unit	Notes/Conditions
Supply voltage[2]	V_{dd}	1.5	3.3	5.5	V	
Storage temperature	T_S	-40		125	°C	
Shock limit (any axis)	g_{max}			5,000	g	
ESD		-2		+2	kV	Human body model

[1] Maximum limits the device will withstand without damage

[2] With 1.5V-2.5V excitation, full-scale range will be limited. So 3.3V min recommended.

OPERATING RANGES & NOISE - ACCELEROMETER

(Unless otherwise specified, all parameters are measured at 24°C @ 3.3V applied)

Measurement Range (g)	Sensitivity mV/g	Non-Linearity (%FSO)	Residual Noise[1] (mg RMS)	Spectral Noise (mg/√Hz)			
				10Hz	100Hz	1kz	10kHz
±25	50.0	±2	2.9	0.15	0.07	0.03	0.02
±50	25.0	±2	5.9	0.29	0.13	0.05	0.05
±100	12.5	±2	11.7	0.58	0.27	0.09	0.09
±200	6.3	±2	23.2	1.16	0.53	0.18	0.18
±500	2.50	±2	58.5	2.92	1.34	0.52	0.45
±1000	1.25	±2	117	5.84	2.68	1.04	0.90
±2000	0.63	±2	234	11.7	5.36	2.08	1.80

[1] 2Hz to 10 kHz

ELECTRICAL SPECIFICATIONS

(Unless otherwise specified, all parameters are measured at 24°C @ 3.3V applied)

Parameters	Symbol	Min	Typ	Max	Unit	Notes/Conditions
Excitation voltage	V_{dd}	3.3		5.5	Vdc	
Zero g output voltage			$V_{dd}/2$			50% of applied voltage
Average supply current	I_{avg}		200		µA	
Output impedance	R_{out}			100	Ω	
Warm-up time				1	Sec	

OPERATING SPECIFICATIONS - ACCELEROMETER

(Unless otherwise specified, all parameters are measured at 24°C @ 3.3V applied)

Parameter	Symbol	Min	Typ	Max	Unit	Notes/Conditions
Full scale output			±1.25		V	
0.0g output voltage (bias V)			$V_{dd}/2$			
Frequency response		6		10k	Hz	±1db
Frequency response		2		15k	Hz	±3db
Resonant frequency		30k			Hz	
Transverse sensitivity				8	%	All Axes
Calibration		CS-SENS-0100 NIST Traceable Amplitude Calibration at 80Hz All parts are shipped with calibration data				

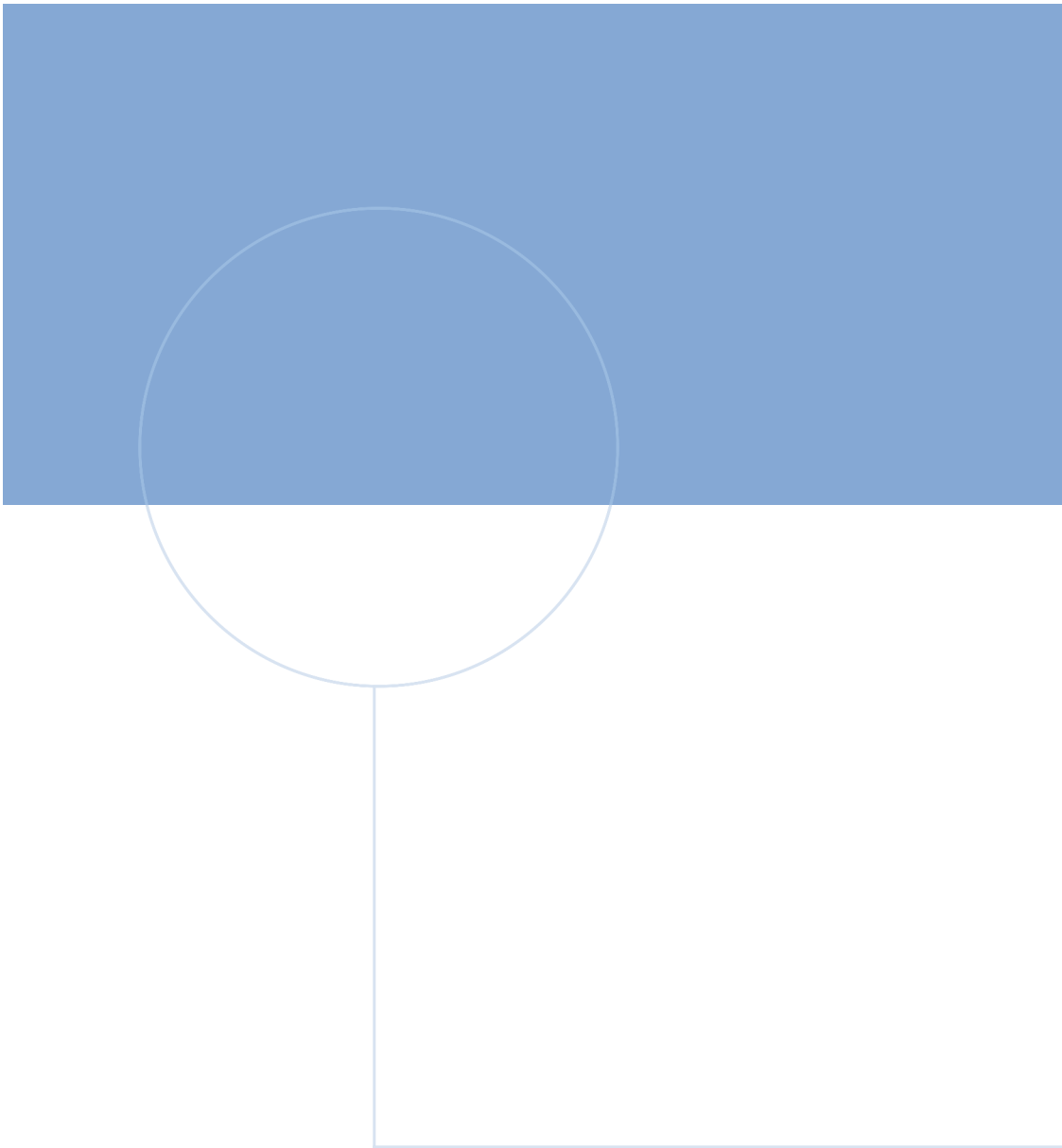

NTNU

Norwegian University of
Science and Technology